Long-Range Connections Synchronize Rather Than Spread Intrathalamic Oscillations: Computational Modeling and In Vitro Electrophysiology

Vikaas S. Sohal and John R. Huguenard

J Neurophysiol 80:1736-1751, 1998.

You might find this additional info useful...

This article cites 34 articles, 19 of which can be accessed free at:
/content/80/4/1736.full.html#ref-list-1

This article has been cited by 5 other HighWire hosted articles

The Sleep Slow Oscillation as a Traveling Wave
Marcello Massimini, Reto Huber, Fabio Ferrarelli, Sean Hill and Giulio Tononi
J. Neurosci., August 4, 2004; 24 (31): 6862-6870.
[Abstract] [Full Text] [PDF]

Interactions Between Membrane Conductances Underlying Thalamocortical Slow-Wave Oscillations
A. DESTEXHE and T. J. SEJNOWSKI
Physiol Rev, October , 2003; 83 (4): 1401-1453.
[Abstract] [Full Text] [PDF]

Actions of U-92032, a T-Type Ca^{2+} Channel Antagonist, Support a Functional Linkage Between I_T and Slow Intrathalamic Rhythms
Darrell M. Porcello, Stephen D. Smith and John R. Huguenard
J Neurophysiol, January 1, 2003; 89 (1): 177-185.
[Abstract] [Full Text] [PDF]

Neuron: A Tool for Neuroscientists
M. L. Hines and N. T. Carnevale
Neuroscientist, April , 2001; 7 (2): 123-135.
[Abstract] [PDF]

Reciprocal Inhibitory Connections Regulate the Spatiotemporal Properties of Intrathalamic Oscillations
Vikaas S. Sohal, Molly M. Huntsman and John R. Huguenard
J. Neurosci., March 1, 2000; 20 (5): 1735-1745.
[Abstract] [Full Text] [PDF]

Updated information and services including high resolution figures, can be found at:
/content/80/4/1736.full.html

Additional material and information about ***Journal of Neurophysiology*** can be found at:
http://www.the-aps.org/publications/jn

This information is current as of April 2, 2015.

Journal of Neurophysiology publishes original articles on the function of the nervous system. It is published 12 times a year (monthly) by the American Physiological Society, 9650 Rockville Pike, Bethesda MD 20814-3991. Copyright © 1998 by the American Physiological Society. ISSN: 0022-3077, ESSN: 1522-1598. Visit our website at http://www.the-aps.org/.

Downloaded from on April 2, 2015

Long-Range Connections Synchronize Rather Than Spread Intrathalamic Oscillations: Computational Modeling and In Vitro Electrophysiology

VIKAAS S. SOHAL AND JOHN R. HUGUENARD
Department of Neurology and Neurological Sciences, Stanford University School of Medicine, Stanford, California 94305-5122

Sohal, Vikaas S. and John R. Huguenard. Long-range connections synchronize rather than spread intrathalamic oscillations: computational modeling and in vitro electrophysiology. *J. Neurophysiol.* 80: 1736–1751, 1998. A thalamic network model was developed based on recent data regarding heterogeneous thalamic reticular (RE) cell axonal arborizations that indicate at least two projection patterns, short-range cluster projections and long-range diffuse projections. The model was constrained based on expected convergence and the biophysical properties of RE and thalamocortical (TC) cells and their synapses. The model reproduced in vitro synchronous slow (3-Hz) oscillatory activity and the known effects of T-channel blockade and cholecystokinin (CCK) application on this activity. Whereas previous models used the speed at which ≈3-Hz oscillations propagate in vitro to infer the spatial extent of intrathalamic projections, we found that, so long as the γ-aminobutyric acid-B synaptic conductance was adjusted appropriately, a network with only short-range projections and another network with both short- and long-range projections could both produce physiologically realistic propagation speeds. Although the ≈3-Hz oscillations propagated at similar speeds in both networks, phase differences between oscillatory activity at different locations in the network were much smaller in the network containing both short- and long-range projections. We measured phase differences in vitro and found that they were similar to those that arise in the network containing both short- and long-range projections but are inconsistent with the much larger phase differences that occur in the network containing only short-range projections. These results suggest that, although they extend much further than do short-range cluster projections, long-range diffuse projections do not spread activity over greater distances or increase the speed at which intrathalamic oscillations propagate. Instead, diffuse projections may function to synchronize activity and minimize phase shifts across thalamic networks. One prediction of this hypothesis is that, immediately after a collision between propagating oscillations, phase gradients should vary smoothly across the thalamic slice. The model also predicts that phase shifts between oscillatory activity at different points along a thalamic slice should be unaffected by T-channel blockers and decreased by suppression of synaptic transmission or application of CCK.

INTRODUCTION

The thalamus participates in a variety of cortical rhythms including 7- to 14-Hz sleep spindles and absence seizures (for a review see Steriade et al. 1993). The most direct evidence for thalamic involvement arises from lesioning studies. Sleep spindles can be demonstrated in the thalamus after decortication in cats (Morison and Basset 1945) yet are absent from cortical tissue that was isolated from thalamus (Burns 1950). Although it was shown that cortical feedback does play an important role in spindle coherence (Contreras et al. 1996), it is clear that spindle generation is largely a thalamic phenomenon. In fact, the thalamus generates spindlelike oscillations in vitro (Bal et al. 1995a,b; Kim et al. 1995; Ulrich and Huguenard 1997; von Krosigk et al. 1993), and the γ-aminobutyric acid-A ($GABA_A$) antagonist bicuculline transforms these oscillations into more synchronized ≈3-Hz oscillations (Bal et al. 1995a,b; Ulrich and Huguenard 1997; von Krosigk et al. 1993) that resemble the thalamic neuronal activity observed during experimental absence seizures (reviewed by Huguenard and Prince 1997). These observations suggest that thalamic circuitry may contribute to the generation of pathological oscillations in vivo.

A combination of in vivo (Steriade et al. 1985) and in vitro recordings (Bal et al. 1995a,b; Huguenard and Prince 1994; von Krosigk et al. 1993) and computational modeling (Destexhe et al. 1996a; Golomb et al. 1996) elucidated a probable mechanism for the spindlelike and more synchronized ≈3-Hz oscillations; bursts in thalamic reticular (RE) cells elicit inhibitory postsynaptic potentials (IPSPs) followed by rebound bursts in thalamocortical (TC) cells. These bursts in TC cells then elicit excitatory postsynaptic potentials (EPSPs) that produce bursts in RE cells, causing the cycle to repeat.

Computational models have also shown how the propagation of both types of oscillations, observed in vitro (Kim et al. 1995), could result from the recruitment of additional cells in each cycle by divergent connections between RE and TC cells (Destexhe et al. 1996a; Golomb et al. 1996). These models used the speed at which oscillations propagate in vitro to infer that connections between RE and TC cells contact cells within a region ~100 μm in radius (Destexhe et al. 1996a) or that the sum of the radius of RE to TC connections and that of TC to RE connections is ~100 μm (Golomb et al. 1996).

A recent anatomic study found that the axonal arborizations of some RE cells extend over a radius of ~100 μm (''cluster'' cell) (Cox et al. 1996), consistent with the aforementioned predictions about connections from RE to TC cells (Destexhe et al. 1996a; Golomb et al. 1996). However, the same anatomic study also found an approximately equal number of RE cells whose axonal arborizations extend over radii of several hundred microns (diffuse projection cells), and another study found that certain physiological properties,

0022-3077/98 $5.00 Copyright © 1998 The American Physiological Society

Downloaded from on April 2, 2015

such as synaptic strength, are correlated with the size of an RE cell's axonal arborization (Cox et al. 1997b). The combined findings of widely distributed apparent synaptic contacts and the weak synaptic coupling strength suggested the diffuse cells could not powerfully influence individual TC cells but rather would only exert a weak (''tickler'') effect. The relatively large distances over which tickler connections extend are not in accord with estimates based on propagation speeds observed in vitro, nor are the functional implications of tickler connections or of the physiological differences among RE to TC connections known.

Here we employ a combination of computational modeling and in vitro electrophysiology to study the functional implications of long-range tickler connections for thalamic circuits. We focus on how these connections affect the propagation speed and degree of synchrony of the ≈3-Hz oscillations in the bicuculline-treated thalamic slice. We show that a network model of this preparation can exhibit similar, physiologically realistic propagation speeds in the presence and absence of long-range tickler connections. We also compare phase differences across the slice, during oscillations in vitro, and in network models with and without long-range tickler connections. We find that only network models that include long-range tickler connections can reproduce the relatively small phase differences observed in vitro. These findings suggest that the primary function of long-range tickler connections (Cox et al. 1996) may be synchronizing activity and minimizing phase shifts across thalamic networks rather than spreading activity over greater distances (and at greater speeds).

METHODS

Model neurons

We studied a network model that included 64 TC and 64 RE neurons. These were based on earlier models of TC (Huguenard and McCormick 1992; McCormick and Huguenard 1992) and RE neurons (Destexhe et al. 1996b). Each neuron was modeled as a single compartment. V_T and V_R, the membrane potentials of TC and RE cells, respectively, evolved according to

$$C_m V_T = -g_L(V_T - E_L) - I_T - I_h I_K - I_{Na} - I_{GABA\text{-}B} \quad (1)$$

$$C_m V_R = -g_L(V_R - E_L) - I_{Ts} - I_K - I_{Na} - I_{AMPA} \quad (2)$$

where the specific capacitance of the membrane, C_m, equals 1 μF/cm^2, g_L is the leak conductance, E_L is the reversal potential of the leak current, I_T and I_{Ts} are low-threshold calcium currents, I_h is the hyperpolarization-activated cation current, I_K and I_{Na} are the potassium and sodium currents underlying action potentials, $I_{GABA\text{-}B}$ is the inhibitory postsynaptic current mediated by $GABA_B$ receptors, and I_{AMPA} is the excitatory postsynaptic current mediated by α-amino-3-hydroxy-5-methyl-4-isoxazolepropionic acid (AMPA) receptors. Parameters and kinetics of intrinsic currents are described in APPENDIX A.

As in previous models, the total membrane area was 29,000 μm^2 for TC cells (Destexhe et al. 1996a; McCormick and Huguenard 1992) and 14,260 μm^2 for RE cells (Destexhe et al. 1996a).

AMPA currents

We used a first-order activation scheme (Destexhe et al. 1996a; Wang and Rinzel 1992) for AMPA receptor-mediated synaptic currents. At each postsynaptic site, R, the fraction of activated AMPA receptors evolved according to

$$\dot{R} = \alpha[C](1 - R) - \beta R \quad (3)$$

where $\alpha = 0.94$ ms/mM, $\beta = 0.18$ ms^{-1}, and $[C]$, the concentration of transmitter in the synaptic cleft, was 0.5 mM during a 0.3-ms interval after each presynaptic spike and 0 otherwise.

$GABA_B$ currents

Initially, to simulate $GABA_B$ receptor-mediated synaptic currents, we followed the assumption of Destexhe and Sejnowski (1995) that each K^+ channel only opens after binding multiple G-protein subunits. In such a model, K^+ current is a supralinear function of the concentration of G-protein subunits, so the concentration of G-protein subunits must decay much more slowly than does the K^+ current. By allowing G-protein subunits to accumulate, this slow decay produces significant temporal summation between $GABA_B$ responses, making it difficult to reproduce the type of paired-pulse depression of $GABA_B$ responses observed in vitro (Otis et al. 1993).

Therefore we assumed that the ''$GABA_B$ response,'' i.e., the postsynaptic K^+ current, depends linearly on postsynaptic $GABA_B$ receptor activation. This assumption is supported by two pieces of experimental evidence. First, during a paired pulse experiment, the time courses of the first and second $GABA_B$ responses are the same (Otis et al. 1993). In contrast, if there is a nonlinear step between $GABA_B$ receptor activation and the opening of K^+ channels, then residual second messenger, activated $GABA_B$ receptors, etc., present during the second response should change the relative contributions of fast and slow components of decay. Second, the ratio of the evoked $GABA_A$ and $GABA_B$ responses in ventrobasal thalamus (VB) neurons is fixed over a range of stimulation intensities (Huguenard and Prince 1994). These two experimental observations suggest that there exists a physiological regime in which the $GABA_B$ response can be accurately simulated with a linear model.

This model is assumed to operate within that regime so that every $GABA_B$ response has the same time course. The time course consists of a fourth-power monoexponential rise and a biexponential decay (Otis et al. 1993; Ulrich and Huguenard 1996a). The amplitude of each $GABA_B$ response equaled the product of the maximum postsynaptic $GABA_B$ conductance ($g_{GABA\text{-}B}$), the fraction of presynaptic sites that released transmitter, and the fraction of postsynaptic $GABA_B$ receptors that were unoccupied at the time of transmitter release.

Probabilistic GABA release and paired-pulse depression

Whenever a presynaptic RE cell spiked, each of its axon terminals released γ-aminobutyric acid (GABA) with a certain probability. Activation of presynaptic $GABA_B$ receptors on RE cells (Ulrich and Huguenard 1996a) produces paired-pulse depression of $GABA_A$ IPSPs and may similarly affect $GABA_B$ responses, as observed in dentate gyrus (Otis et al. 1993). To model this phenomenon, the probability of GABA release decreased as a result of previous release from the same synapse.

The time course of postsynaptic $GABA_B$ currents and the methods for calculating postsynaptic $GABA_B$ receptor occupancy and the probability of GABA release are given in APPENDIX A.

Network architecture

As mentioned in the INTRODUCTION, this model represents a thalamic slice that was treated with bicuculline and therefore does not include any $GABA_A$ synapses. Instead, network connectivity consists solely of $GABA_B$ synapses from RE cells to TC cells and AMPA synapses from TC cells to RE cells. For simplicity, we did

Downloaded from on April 2, 2015

not model $GABA_B$ synapses between RE cells, which are extremely weak (Ulrich and Huguenard 1996a).

Following earlier models (Destexhe et al. 1996a; Golomb et al. 1996), this network has a one-dimensional architecture in which neurons are distributed evenly along a straight line in two layers (one layer consists of RE cells and the other consists of TC cells). The network models a slice 3.2 mm in length, so the spacing between neighboring cells corresponds to 50 μm along a thalamic slice. On the basis of anatomic evidence that connections between RE and TC cells are topographic (Agmon et al. 1995; Mitrofanis and Guillery 1993; but see Jones 1985), the model assumes that an RE cell located at position x along the line contacts TC cells located within some radius of x and vice versa.

Connections from TC cells to RE cells

Retrograde labeling suggests that the axons of mouse TC cells from different barreloids remain well segregated in the thalamic RE nucleus and that the axonal arborization from a single barreloid has a radius $<$50 μm in the thalamic RE nucleus (Agmon et al. 1995). TC cells appear to make synaptic contacts on the somata of RE cells (Ide 1982), but, even if TC cells do contact the dendritic arbors of RE cells, these arbors typically have radii $<$100 μm (Cox et al. 1996; Lübke 1993; Scheibel and Scheibel 1966; Spreafico et al. 1991). On the basis of these observations, the model included connections from TC cells to RE cells within a 50-μm radius. Unless otherwise noted, the total postsynaptic AMPA conductance on each RE cell was $\bar{g}_{AMPA}$ = 150 nS (although the fraction of AMPA receptors was never $>$0.2, which corresponds to an effective $\bar{g}_{AMPA}$ of 30 nS). Therefore the conductance at each AMPA synapse was proportional to $1/n$ where n is the total number of AMPA synapses on the postsynaptic cell.

Connections from RE cells to TC cells

RE cells can be separated into groups that have anatomically and physiologically different projections to TC cells (Cox et al. 1996, 1997b). One group has projections to TC cells that are strong and contain a high density of axonal swellings but are restricted to a relatively small region (cluster connections). In contrast, the other group has connections to TC cells that are weaker and contain a relatively low density of axonal swellings but extend over a much more widespread region (diffuse or tickler connections). Viewed on the basis of these properties, RE cells appear to fall into distinct categories rather than along a continuum, and these categories appear to contain approximately equal numbers of cells (Cox et al. 1996, 1997b).

The somatic and dendritic properties of RE cells that send different types of connections (tickler or cluster) to TC cells appear to be similar (Cox et al. 1996). As a result, the model was able to represent the heterogeneity of axonal arborizations of RE cells among TC cells simply by including two sets of connections from RE cells to TC cells without having to include distinct populations of RE cells. Therefore each model RE cell made two sets of connections onto TC cells. One set, representing tickler connections, only made a few synaptic contacts (6) (Cox et al. 1997b) with each postsynaptic TC cell and elicited relatively weak postsynaptic $GABA_B$ currents but contacted TC cells over a relatively large radius (500 μm) (Cox et al. 1996). The other set, representing cluster connections, made many synaptic contacts (257) (Cox et al. 1997b) with each postsynaptic TC cell and elicited relatively strong postsynaptic $GABA_B$ currents but only contacted TC cells over a relative small radius (100 μm) (Cox et al. 1996).

On the basis of the physiological evidence reviewed in APPENDIX A, the ratio between the $GABA_B$ conductance postsynaptic to tickler connections and the $GABA_B$ conductance postsynaptic to cluster connections was determined by the ratio between the areas of the axonal arborizations of tickler and cluster cells. Furthermore, the $GABA_B$ conductance at each tickler synapse was proportional to $1/n_{tickler}$, where $n_{tickler}$ is the number of tickler synapses on a TC cell. Similarly, the $GABA_B$ conductance at each cluster synapse was proportional to $1/n_{cluster}$, where $n_{cluster}$ is the number of cluster synapses on a TC cell. Thus three parameters, the total $GABA_B$ conductance on a TC cell ($g_{GABA\text{-}B}$) and the radii of tickler and cluster connections, determine the $GABA_B$ conductances at every tickler and cluster synapse on that TC cell. As described in the RESULTS, we tested many values of $g_{GABA\text{-}B}$ and choose the one for which simulated oscillations propagated at speeds similar to those observed in vitro. Then we compared results from simulations in which tickler connections had the radius measured anatomically (500 μm) to those from simulations in which tickler connections had the same radius as cluster connections (100 μm). Because all other parameters were physiologically constrained, we could then deduce possible functions of long-range (500 μm in radius) tickler connections.

Computational methods

All simulations were run with NEURON (Hines and Carnevale 1997) at a temperature of 37°C and with a time step of 0.1 ms. Every simulation began with a 500-ms delay period preceding stimulation of any neurons that allowed window currents, etc., to reach steady state. This delay period is not shown in any figures. Distributions of pseudorandom variables were always initialized with the same seed value, allowing us to compare results from networks with different parameters but the same ''random'' initial conditions. To check for finite-size effects, we repeated our simulations with a network of 128 each TC and RE cells representing a thalamic slice of the standard length (so connections from one cell contacted twice as many cells as in the standard network). We also checked for edge effects by repeating our simulations with a network of 128 each TC and RE cells representing a thalamic slice that was twice the standard length (so connections from one cell contacted the same number of cells as in the standard network).

In vitro slice recordings

Slice experiments were performed as previously described (Huguenard and Prince 1994). Rat pups of either sex, aged 14–18 days (p14–p18) were anesthetized (50 mg/kg pentobarbital) and decapitated, and the brains were rapidly removed and placed in chilled (4°C) low-Ca, low-Na slicing solution consisting of (in mM) 234 sucrose, 11 glucose, 24 $NaHCO_3$, 2.5 KCl, 1.25 NaH_2PO_4, 10 $MgSO_4$ and 0.5 $CaCl_2$, equilibrated with a mixture of 95% O_2-5% CO_2. Horizontal slices 400 μm thick were obtained with a vibratome (TPI, St. Louis). The slices were incubated in 30°C oxygenated saline before being placed in a modified (partially submerged) interface recording chamber. Slices were maintained at 34 $\pm$ 1°C in the recording chamber and remained viable for several hours under these conditions. The superfusion solution consisted of (in mM) 126 NaCl, 26 $NaHCO_3$, 2.5 KCl, 1.25 NaH_2PO_4, 0.63 $MgCl_2$, 2 $CaCl_2$, 0.01 bicuculline methiodide (BMI), and 10 glucose. Extracellular stimuli were delivered through a pair of 1- to 10-MΩ tungsten electrodes (FHC, Maine) glued together with a separation of about 100 μm. Extracellular unit and multiunit recordings were obtained with 5- to 10-MΩ tungsten electrodes and normally filtered between 100 and 3 KHz.

RESULTS

Here we briefly describe the results of extracellular recording from thalamic slices and then describe in detail simulations of this and other experimental data with our network model. Finally, we quantitatively compare the experimental

Downloaded from on April 2, 2015

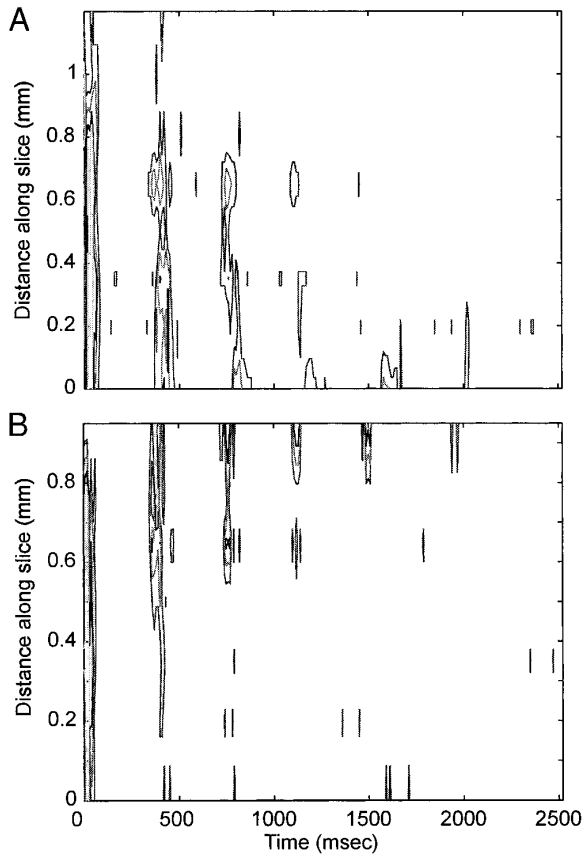

FIG. 1. Synchronous, slow (≈3-Hz) intrathalamic oscillations in vitro, evoked by stimulation of internal capsule. Long-lasting slow oscillations are promoted by blocking γ-aminobutyric acid-A ($GABA_A$) synaptic responses with bicuculline methiodide (Cox et al. 1997a; Huguenard and Prince 1994; Ulrich and Huguenard 1997). *A*: contour plot of extracellular multiunit activity at several locations in reticular (RE) cells. *B*: contour plot of extracellularly activity from thalamocortical (TC) cells at several locations in ventrobasal thalamus (VB). Oscillatory activity persisted for ~2 s. Activity is expressed as the firing frequency per unit time (ratemeter-type output) normalized by the maximum firing frequency at that location. Each contour corresponds to an incrementally higher firing frequency. These recordings were not simultaneous, but in all cases *time 0* is the time at which internal capsule was stimulated.

results with results obtained with two network models with different parameters. In the following section, we focus on results from the standard network, having 64 TC cells and 64 RE cells, because results from the networks with 128 TC cells and 128 RE cells were qualitatively and quantitatively similar to these.

Slow, synchronized intrathalamic oscillations in vitro

Figure 1, *A* and *B*, shows contour plots of extracellularly recorded activity from RE and TC cells, respectively, as functions of time (running horizontally) and distance along the slice (running vertically). These figures show that, as in previous experiments (Huguenard and Prince 1994), indirect excitation of RE cells via stimulation of internal capsule elicits ≈3-Hz oscillations. They also show that these oscillations remain highly synchronized across widely separated RE and TC cells.

Interactions between RE and TC cells produce synchronized network oscillations

As in Fig. 1, in earlier in vitro studies (Bal et al. 1995a,b; Huguenard and Prince 1994; Kim et al. 1995; von Krosigk et al. 1993) and earlier models (Destexhe et al. 1996a; Golomb et al. 1996), interactions between RE and TC cells produce synchronized oscillations at ≈3 Hz in our network model. Figure 2*A* shows a contour plot of RE cell activity (i.e., the spike rate of each RE cell, computed with 10-ms wide bins) as a function of time (horizontal axis) and distance along the slice (vertical axis). Figure 2*B* shows an analogous contour plot of TC cell activity. Figure 2*C* plots membrane potential versus time for an RE cell at the center of the slice, and Fig. 2*D* plots the membrane potential versus time for the corresponding TC cell.

The oscillations are initiated by bursts in RE cells; to simulate the indirect excitation of RE cells via stimulation of internal capsule, we randomly excited one-third of the RE cells above the burst threshold. These bursts in RE cells elicit slow $GABA_B$ receptor-mediated IPSPs followed by rebound bursts (resulting from the deinactivation of I_T by the IPSPs) in TC cells (shown in Fig. 2*D*). Bursts in TC cells elicit fast EPSPs that produce bursts in RE cells (shown in Fig. 2*C*), causing the cycle to repeat. As a result of this cycle of events, in which TC cells' bursts elicit bursts in RE cells with short latency whereas RE cells' bursts only elicit bursts in TC cells after a prolonged IPSP, TC cell activity is slightly phase-advanced relative to RE cell activity during the simulated oscillations shown in Fig. 2. This is consistent with the phase relationship shown in Fig. 1 and found in earlier in vitro studies (Bal et al. 1995a,b; von Krosigk et al. 1993). For the network shown, $g_{GABA\text{-}B}$ = 31.5 nS (although the fraction of $GABA_B$ receptors activated was never >0.7, corresponding to an effective $g_{GABA\text{-}B}$ of 22.1 nS).

Depression of GABA release causes oscillations to terminate

The oscillations shown in Figs. 1 and 2 lasted ~2 s, similar to the duration of slow, synchronous oscillations observed in vitro (Bal et al. 1995a,b; Huguenard and Prince 1994; Kim et al. 1995; von Krosigk et al. 1993). In the network model, IPSPs in TC cells gradually waned, as shown in Fig. 2*D*, because of the presynaptic suppression of GABA release, until they were no longer sufficiently hyperpolarizing to elicit rebound bursts, and the oscillation terminated. Figure 3, *A* and *B*, shows contour plots of activity in a network, identical to those depicted in Fig. 2, except that the probability of GABA release does not decrease. Whereas the oscillations shown in Figs. 1 and 2 terminated after ~2 s, the network activity shown in Fig. 3 continued to oscillate for the duration of the simulation (3 s).

Although the depression of GABA release implemented in this model could terminate oscillations, it did not produce a significant refractory period for the generation of oscillations. We found that, 1 s after an oscillation ended, another oscillation could be elicited by stimulating RE cells at the same location (cf. Kim et al. 1995).

Downloaded from on April 2, 2015

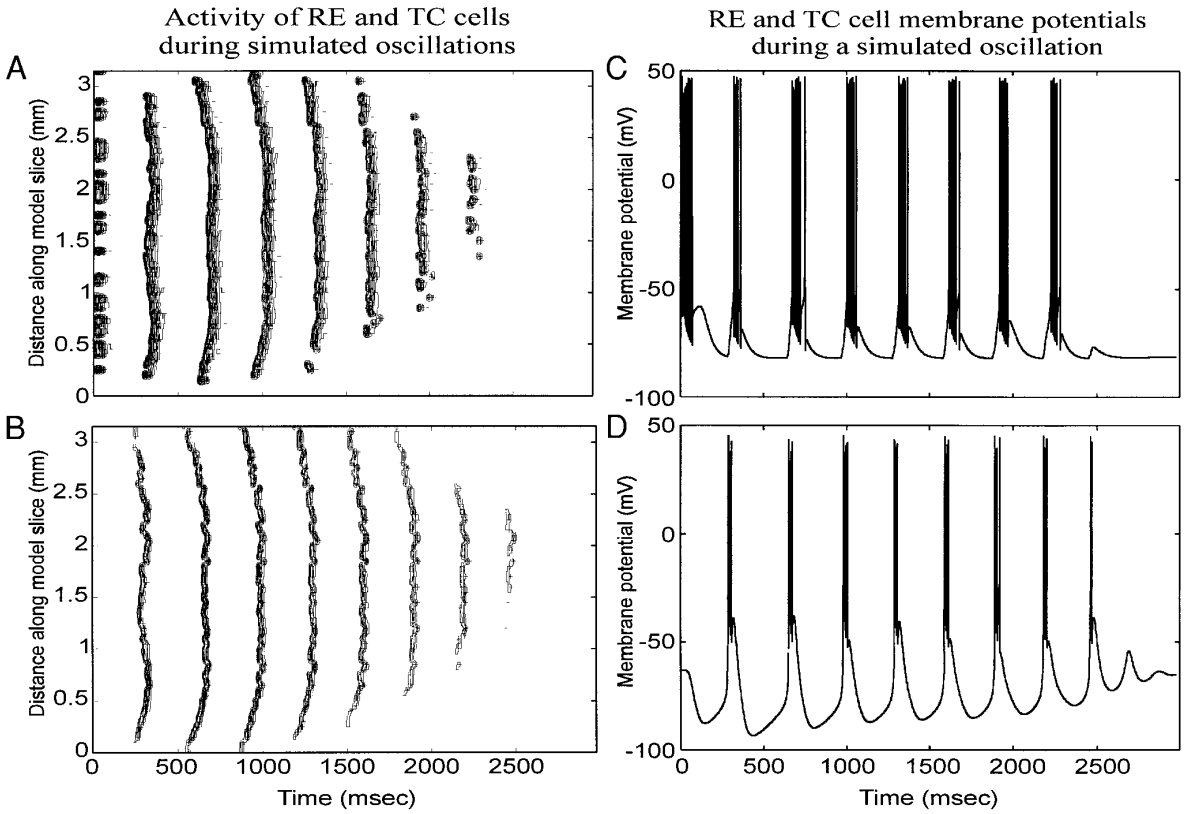

FIG. 2. Synchronous, slow (≈3-Hz) oscillations in the network model. *A*: contour plot of the activity of 64 RE cells as a function of time and distance along the model slice. *B*: similar plot of activity in 64 TC cells. As in Fig. 1, oscillatory activity persisted for ~2 s. Activity is expressed as firing frequency. To simulate the indirect excitation of RE cells via stimulation of internal capsule, 1/3 of the RE cells were excited above the burst threshold at *time 0*. *C*: plot of the membrane potential vs. time for an RE cell at the center of the model slice. The RE cell bursts once per cycle, and the number of spikes per burst is similar to that observed during bicuculline-induced slow oscillations in vitro. *D*: plot of the membrane potential vs. time for a TC cell at the center of the model slice. Again, the TC cell bursts once per cycle, and the number of spikes per burst is similar to that observed in vitro. As the oscillation progresses, GABA release declines because of the activation of presynaptic $GABA_B$ autoreceptors on RE cells (not shown). Consequently, the peak deflection of inhibitory postsynaptic potentials (IPSPs) become less hyperpolarized, as observed in vitro, until the IPSPs are too weak to sustain the oscillation. $\bar{g}_{GABA\text{-}B}$ was 30.5 nS [$\bar{g}_{GABA\text{-}B}$ (tickler) = 21.8 nS and $\bar{g}_{GABA\text{-}B}$(cluster) = 8.7 nS] and $\bar{g}_{AMPA}$ was 150 nS.

Blocking T-channels reduces the duration and increases the period of oscillations

We simulated the effects of T-channel blockers by reducing P_{Ts} and P_T, the permeabilities of T currents in RE and TC cells, respectively (the network was otherwise identical to that represented by Fig. 2). Figure 4 includes two contour plots that compare RE cell activity before and after a 25% reduction in P_T and P_{Ts}. Figure 4 also plots the period, duration, and phase shift (this phase shift will be defined and discussed later) of ≈3-Hz oscillations versus the percent reduction in P_T and P_{Ts}. These plots demonstrate that, as in experiments (Huguenard and Prince 1994; Smith and Huguenard 1996), modest T-channel blockade shortens the duration and reduces the period of the slow, synchronous oscillations. For example, oscillations in the control network had a period of 328 ms and lasted eight cycles, whereas after 25% T-current blockade the period was 363 ms and the oscillations lasted five cycles.

This finding is easily understood. As observed experimentally (Bal et al. 1995a) and shown in Fig. 2, *C* and *D*, most of a cycle is spent in the time it takes IPSPs in TC cells to decay, producing a rebound burst. When some T-channels are blocked, the threshold for a Ca^{2+} spike (a dynamic variable) (see Ulrich and Huguenard 1996b) becomes more depolarized. As a result, TC cells reach threshold later, prolonging each cycle of the oscillation. Similarly, when some T-channels are blocked, stronger IPSPs are required to elicit rebound bursts. As a result, IPSPs fall below this critical strength, and the oscillation terminates earlier.

Suppression of synaptic transmission shortens both the duration and period of oscillations

We also simulated the suppression of intrathalamic synaptic transmission by reducing both synaptic conductances, $\bar{g}_{GABA\text{-}B}$ and $\bar{g}_{AMPA}$ (the network was otherwise identical to that represented by Fig. 2). Figure 5 includes two contour plots that compare RE cell activity before and after suppressing synaptic strength by 25% and also plots period, duration, and phase shift versus percent suppression of synaptic strength. Suppression of synaptic strength shortened both the duration and period of oscillations in network activity. For example, after a reducing synaptic strength by 25%, the duration of oscillations fell from eight cycles to four cycles, and their period fell from 328 to 319 ms.

Downloaded from on April 2, 2015

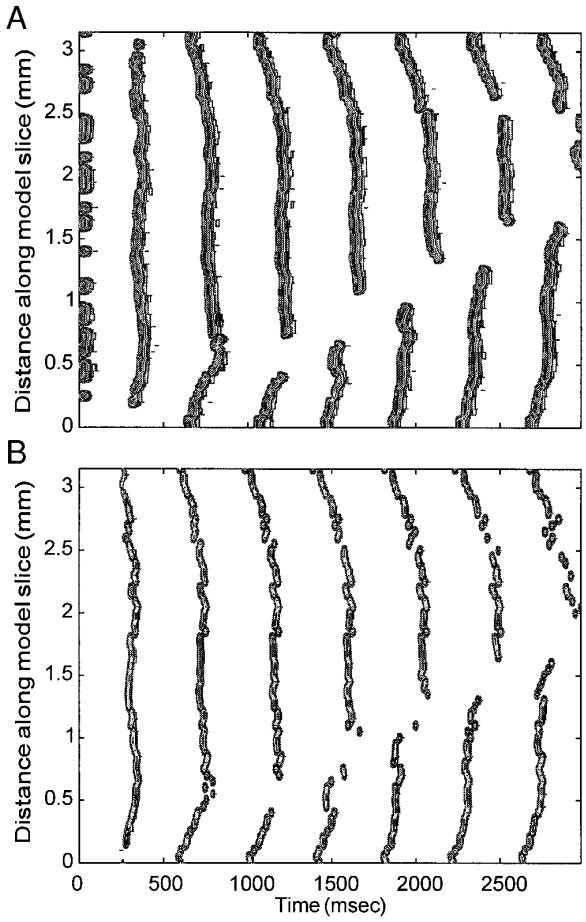

FIG. 3. Simulated oscillations in the absence of paired-pulse depression. *A* and *B* are same as in Fig. 2 except that this network model lacks the $GABA_B$ autoreceptor-mediated suppression of GABA release, which underlies paired-pulse depression. Because paired-pulse depression is absent, oscillatory activity does not terminate and persists for the duration of this simulation (>3 s). Synaptic conductances were the same as in Fig. 2.

This result can be explained as follows. So long as excitatory synaptic transmission remains sufficiently strong to elicit bursts in RE cells, the main consequences of suppressing synaptic transmission result from the weakening of IPSPs in TC cells. Weakening these IPSPs has two possible results. Weaker IPSPs may still hyperpolarize TC cells enough to deinactivate the T current and elicit a rebound burst. In this case, because TC cells are less hyperpolarized by each IPSP, their membrane potentials climb to the threshold for Ca^{2+} spike generation earlier, reducing the length of each cycle. Alternatively, weaker IPSPs may inadequately deinactivate the T current in TC cells, causing the threshold for Ca^{2+} spike generation to rise. As a result, TC cells may take longer to reach this threshold or not reach it at all. In this model, the first effect dominates early on, shortening the period of the oscillation, but the second effect eventually takes over, terminating the oscillation prematurely.

Depolarization of RE cells by CCK has biphasic effects on oscillations

Cholecystokinin (CCK) depolarizes RE cells by decreasing a leak K^+ conductance (Cox et al. 1995). CCK also has biphasic effects on ≈3-Hz thalamic oscillations in vitro; in some slices, low concentrations prolonged these oscillations, but higher doses suppressed these oscillations, whereas in other slices all doses of CCK tested suppressed oscillations (Cox et al. 1997a). We simulated the application of CCK in network models as follows. First, we assumed that the leak current in RE cells was composed of K^+ and Na^+ currents. Assuming that $E_{Na} = +50$ mV and $E_K = -105$, we calculated $g_{leak,K}$ and $g_{leak,Na}$. To simulate varying doses of CCK application, we then increased $g_{leak,K}$ by varying amounts (cf. Sohal and Huguenard 1998).

Figure 6 includes contour plots that show RE cell activity at three different levels of $g_{leak,K}$ and plots of duration, period, and phase shift versus $g_{leak,K}$. Figure 6 demonstrates that, starting from a $g_{leak,K}$ slightly higher than that used in these simulations, reducing $g_{leak,K}$ (and consequently depolarizing RE cells) first increased, then decreased the duration of ≈3-Hz oscillations in the network model. This result reproduces the biphasic effect of CCK on the duration of intrathalamic oscillations in vitro. It also suggests that slices that have a monophasic re-

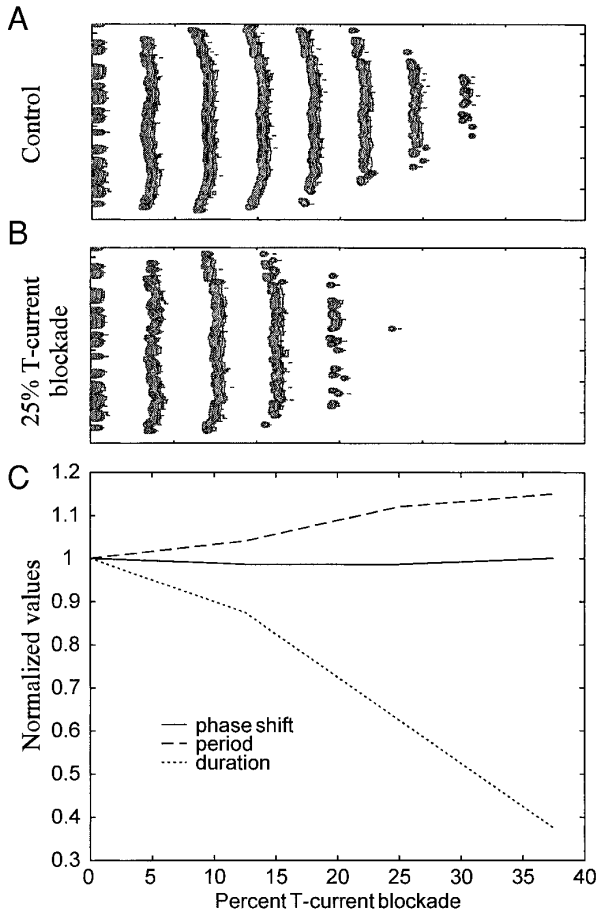

FIG. 4. Effects of T-current blockade on simulated oscillations. The values of P_{Ts} and P_T (the permeabilities of T currents in RE and TC cells) were proportionately reduced in each simulation. Contour plots of RE cell activity before (*A*) and after (*B*) a 25% reduction in P_T and P_{Ts}. *C*: plots of the maximum phase shift (measured on the first cycle of activity after widespread activation of RE cells), oscillation period, and duration of oscillations vs. the percent T-current blockade. All values are normalized by the values in the control network (the network with 0% T-current blockade). Details of contour plots and synaptic conductances were the same as in Fig. 2.

Downloaded from on April 2, 2015

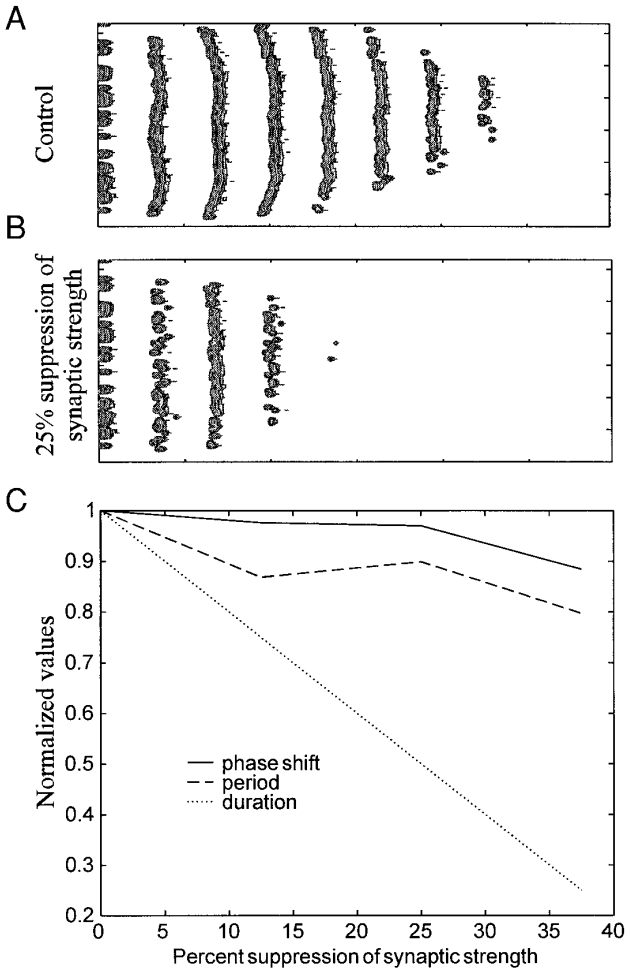

FIG. 5. Effects of suppressing synaptic transmission on simulated oscillations. We simulated suppression of synaptic transmission by reducing both synaptic conductances, $\bar{g}_{\text{GABA-B}}$ and $\bar{g}_{\text{AMPA}}$. Contour plots (see Fig. 2) of RE cell activity before (*A*) and after (*B*) a 25% suppression of synaptic strength (relative to the synaptic strength in Fig. 2). *C*: plots of the maximum phase shift, oscillation period, and duration of oscillations vs. the percent suppression of synaptic transmission. All values are normalized by the values in the control network (the network with 0% suppression of synaptic transmission).

sponse to CCK (shortening of oscillations at all doses) have a lower average $g_{\text{leak,K}}$ than do slices that have a biphasic, dose-dependent response to CCK and that the network model falls in the former category. Furthermore, as observed in vitro (Cox et al. 1997a), low $g_{\text{leak,K}}$ (produced by high doses of CCK) increases the tonic, nonrhythmic, activity of RE cells. Figure 6 also suggests that CCK application should decrease the period of ≈3-Hz oscillations slightly. Although an earlier experiment did verify that oscillations remain in the 2- to 4-Hz range after CCK application (Cox et al. 1997a), small changes in the period were specifically measured. Subsequent analysis of those results indicates that the period is slightly decreased, especially for modest CCK concentrations (e.g., see Fig. 4*B* of Cox et al. 1997a).

Propagation of synchronous oscillations

Slow, synchronous oscillations originating at one point were observed to propagate across thalamic slices (Kim et al. 1995) and one-dimensional network models (Destexhe et al. 1996a; Golomb et al. 1996). Similarly, in this model stimulating a few RE cells located around the center of the model slice created an oscillation that propagates outward in both directions. Figure 7, *A* and *B*, shows the propagation of activity through RE and TC cells, respectively. As described in METHODS, we measured the speed of propagation for many values of $\bar{g}_{\text{GABA-B}}$. In Fig. 7, *A* and *B*, as in earlier simulations, $\bar{g}_{\text{GABA-B}} = 31.5$ nS so that the speed of propagation was 0.28 mm/s, which is within the range of values observed experimentally. APPENDIX A describes how the speed of propagation was calculated.

Propagation of oscillations in the absence of long-range tickler connections

After reducing the radius of tickler cell connections from 500 to 100 μm, while holding constant both the total $GABA_B$ conductance on each TC cell and the ratio between $GABA_B$

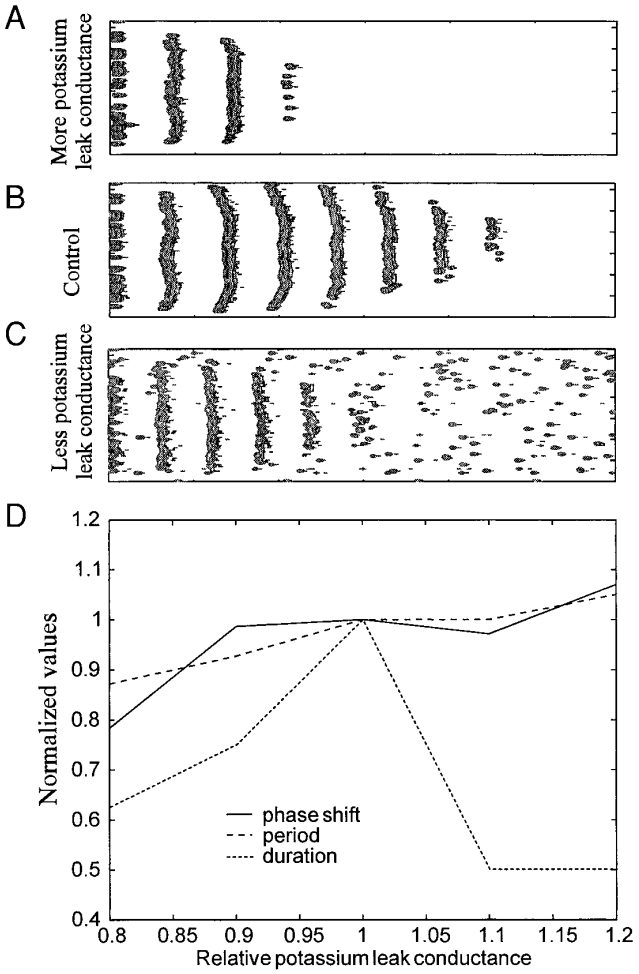

FIG. 6. Effects of cholecystokinin (CCK) on simulated oscillations. On the basis of experimental evidence, we simulated CCK application by reducing the leak potassium conductance, $g_{\text{leak,K}}$, in RE cells. *A–C*: contour plots of RE cell activity for 3 values of $g_{\text{leak,K}}$. *D*: plots of the maximum phase shift, period of oscillations, and duration of oscillations vs. relative $g_{\text{leak,K}}$ (relative $g_{\text{leak,K}} = 1$ corresponds to the value used in the network model). All values are normalized by the values in the control network (the network with $g_{\text{leak,K}} = 1$). Details for contour plots and synaptic conductances are given in Fig. 2.

Downloaded from on April 2, 2015

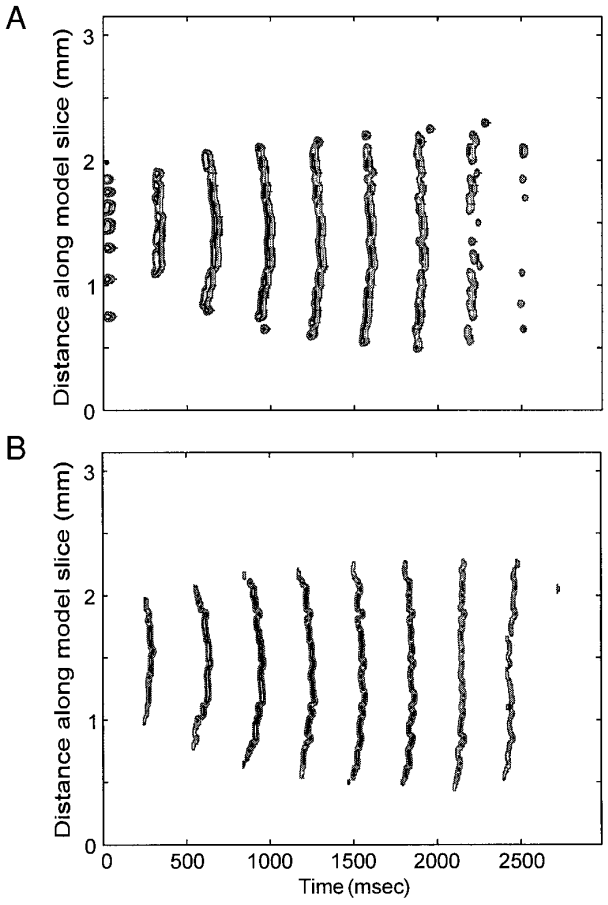

FIG. 7. Propagating oscillations in a network model with long-range tickler connections. Contour plot of concurrent RE cell (*A*) and TC cell (*B*) activity as a function of time and distance along the model slice. An oscillation is elicited by focal stimulation near the center of the slice and subsequently propagates outward at a physiologically realistic speed of 0.28 mm/s. $\bar{g}_{\text{GABA-B}}$ was 30.5 nS, [$\bar{g}_{\text{GABA-B}}$(tickler) = 21.8 nS and $\bar{g}_{\text{GABA-B}}$(cluster) = 8.7 nS] and $\bar{g}_{\text{AMPA}}$ was 150 nS, the radius of connections from TC cells to RE cells was 50 μm, the radius of tickler connections was 500 μm, and the radius of cluster connections was 100 μm. To initiate oscillations, RE cells near the center of the model slice were probabilistically excited above the burst threshold.

conductance postsynaptic to tickler connections and that postsynaptic to cluster connections, focal stimulation still elicits a synchronous, ≈3-Hz oscillation at the center of the slice. However, when $\bar{g}_{\text{GABA-B}}$ = 31.5 nS, this oscillation no longer propagates outward (not shown). However, when the total $GABA_B$ conductance on each TC cell, $\bar{g}_{\text{GABA-B}}$, is increased to 42 nS, then even with these ''short-range'' tickler connections, oscillations elicited by focal stimulation propagate outward from the center of the slice at a speed of 0.24 mm/s. Figure 8, *A* and *B*, displays RE and TC cell activity, respectively, in this network. Thus, we found that by choosing $\bar{g}_{\text{GABA-B}}$ appropriately, both short-range and long-range tickler connections produce synchronous, ≈3-Hz oscillations that propagate at speeds similar to those observed in vitro. However, comparison of Figs. 7 and 8 reveals that the synchronous, ≈3-Hz oscillations are not identical under the two sets of conditions, long-range tickler connections with $\bar{g}_{\text{GABA-B}}$ = 31.5 nS and short-range tickler connections with $\bar{g}_{\text{GABA-B}}$ = 42 nS. Phase differences between distant RE or TC cells seem to be much larger in the latter network (shown in Fig. 8) than in the former (shown in Fig. 7). We sought to quantify this discrepancy to determine which network better matched experimental data.

Long-range, but not short-range, tickler connections produce phase differences that are consistent with experimental measurements

We compared phase differences recorded during in vitro oscillations elicited by stimulation of internal capsule (such as those depicted in Fig. 1) to phase differences that occurred during simulations of these oscillations in networks with either long-range tickler connections and $\bar{g}_{\text{GABA-B}}$ = 31.5 nS (shown in Fig. 2) or short-range tickler connections and $\bar{g}_{\text{GABA-B}}$ = 42 nS (shown in Fig. 9). All other parameters in the two simulated networks were equal. For each simulated

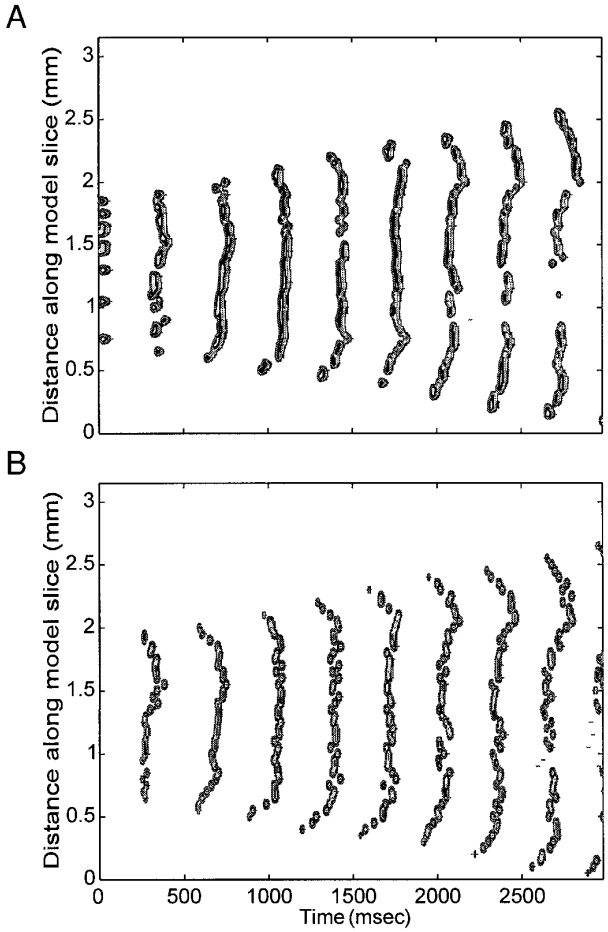

FIG. 8. Propagation of oscillations in a network model without long-range tickler connections. Contour plot of concurrent RE cell (*A*) and TC cell (*B*) activity as a function of time and distance along the model slice. An oscillation is elicited by focal stimulation near the center of the slice (equivalent to that used in Fig. 7) and subsequently propagates outward at a physiologically realistic speed of 0.24 mm/s. Note that, although the speed at which oscillations propagate is similar to that in a network model with long-range tickler connections (shown in Fig. 7), in this case oscillatory activity is much less synchronized across the network. $\bar{g}_{\text{GABA-B}}$ was 42 nS [$\bar{g}_{\text{GABA-B}}$(tickler) = 30 nS and $\bar{g}_{\text{GABA-B}}$(cluster) = 12 nS], the total postsynaptic conductance on each RE cell was $\bar{g}_{\text{AMPA}}$ = 150 nS, the radius of connections from TC cells to RE cells was 50 μm, and the radius of both tickler and cluster connections was 100 μm.

Downloaded from on April 2, 2015

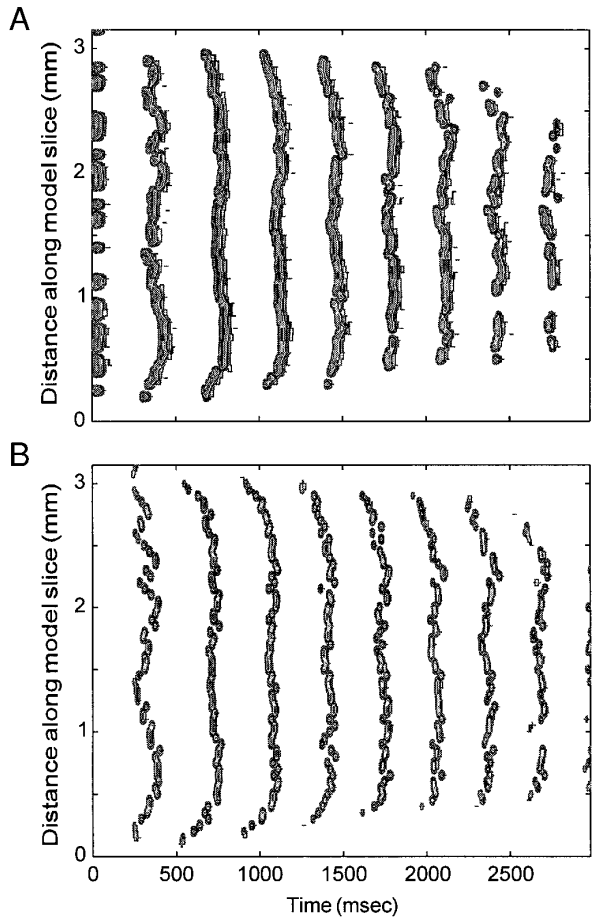

FIG. 9. Synchronous, slow (≈3-Hz) oscillations in a network model without long-range tickler connections. Contour plot of concurrent RE cell (*A*) and TC cell (*B*) activity as a function of time and distance along the model slice. At *time 0*, to simulate the indirect excitation of RE cells via stimulation of internal capsule, ⅓ of the RE cells were excited above the burst threshold. Note that the resulting oscillations are much less synchronized across the network than in a network with long-range tickler connections, shown in Fig. 2. In this network, synaptic conductances were the same as in Fig. 8.

or in vitro oscillation, we calculated the phase difference between TC cell activity at every pair of locations during the first cycle of the oscillation by cross-correlation and found the maximum phase difference. Because extracellular recordings were not made at the edges of the slice and to minimize edge effects, in the network model we only calculated phase differences for cells ≥500 μm away from the edges. During two in vitro oscillations the maximum phase differences were 50 and 60 ms. Simulation of the network with long-range tickler connections resulted in a maximum phase difference of 69 ms, whereas a simulation with short-range connections yielded a maximum phase difference of 151 ms. To provide a sense of just how different these two values were, we found that the maximum phase differences were 68 and 62 ms in the networks with 25% blockade of T-channels and with 25% suppression of synaptic transmission, respectively. This shows that changing the range of tickler connections has a much larger effect on the maximum phase difference than do other manipulations, suppression of synaptic transmission or T-channel blockade, which significantly alter network dynamics. Thus, in response to focal excitation at the center of the slice, both short-range and long-range tickler connections produce oscillations that propagate with approximately equal speeds. However, during simulations of in vitro oscillations elicited by broad stimulation of RE cells, only the network with long-range tickler connections produces phase differences that are similar to those observed in vitro. We also checked for finite-size effects on the maximum phase shift after broad stimulation, with the 256-cell network representing a standard-length slice. In this network the maximum phase shift after stimulation of RE cells (71 ms) was quantitatively similar to that observed in vitro when long-range tickler connections were present but was much larger (123 ms) when they were absent.

We found an analytic expression for the phase of TC cell activity on the first cycle that is derived in APPENDIX B

$$t_{\text{burst}} = \tau_{\text{GABA-B}} \ln\left[\frac{E_{\text{pas}} - E_{\text{GABA-B}}}{E_{\text{pas}} - \theta}\right] + \tau_{\text{GABA-B}} \ln\left[\frac{n\tilde{g}}{1 + n\tilde{g}}\right] \quad (4)$$

where t_{burst} is the time at which the TC cell bursts (relative to the time of RE cells' bursts), $\tau_{\text{GABA-B}}$ is the time constant with which $GABA_B$ postsynaptic potentials decay (assumed to be monoexponential as V_m approaches the burst threshold), E_{pas} is a weighted average of the TC cell's resting membrane potential and the h-current reversal potential, $E_{\text{GABA-B}}$ is the reversal potential of $GABA_B$ synapses, θ is the burst threshold, n is the number of active presynaptic RE cells terminating on this TC cell, and $\tilde{g}$ is the typical postsynaptic conductance activated after a burst in one presynaptic RE cell (divided by the cell's nonsynaptic conductance). This expression was derived with a number of simplifications, including the assumption that connections from RE cells to TC cells are homogeneous. To account for separate tickler and cluster connections, the term $n\tilde{g}$ should be replaced by $n_{\text{tickler}}\tilde{g}_{\text{tickler}} + n_{\text{cluster}}\tilde{g}_{\text{cluster}}$ where n_{tickler} is the number of bursts in presynaptic tickler cells terminating on this TC cell, etc.

Except for small inhomogeneities among neurons, the first term on the right hand sides of *Eq. 4* will be approximately equal in all TC cells. Therefore, assuming that $n\tilde{g} \ll 1$ so that we are far from saturation, the main source of variation in the phase of TC cell bursting, t_{burst}, results from the second term on the right hand side of *Eq. 4*. This term can depend on $\tilde{g}$ and n. Because n is a random variable that represents the number of RE cells presynaptic to a given TC cell that burst, it depends on the spread of connections from RE cells to TC cells and the probability that an RE cell reaches the burst threshold during the initial stimulation. Thus to a first approximation, the variation in the phase of TC cell activity depends in a relatively straightforward way on the synaptic conductance, $\tilde{g}$, and on the radius of connectivity from RE cells to TC cells but does not depend on any other network parameters. This property makes phase shifts during the first cycle of TC cell activity a useful measurement with which to constrain the radius of RE to TC connectivity and the strength of synaptic transmission in our network model.

Collisions among propagating oscillations

Initially out-of-phase oscillations that begin at opposite ends of a thalamic slice in vitro can propagate toward the

Downloaded from on April 2, 2015

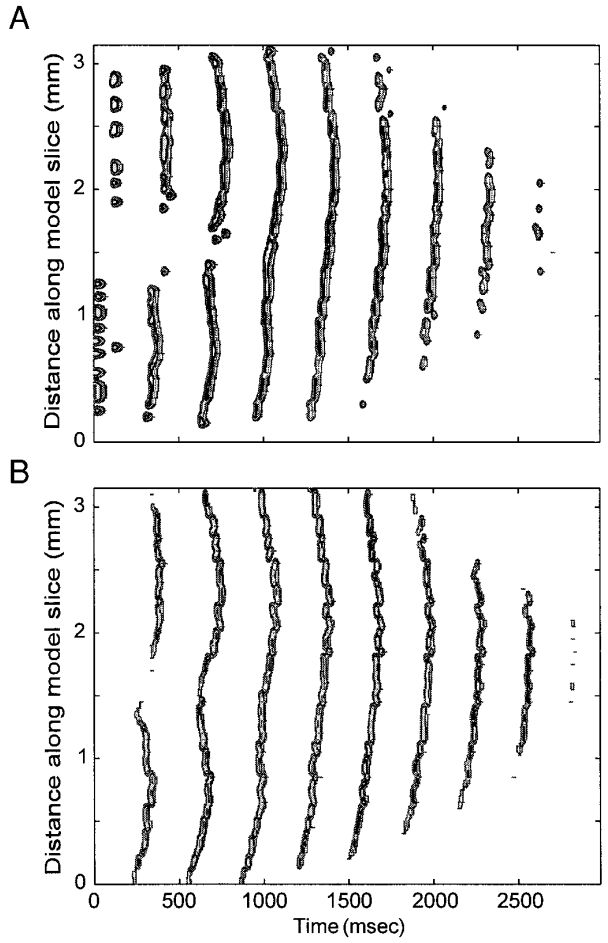

FIG. 10. Colliding oscillations in a network with long-range tickler connections. Contour plot of concurrent RE cell (*A*) and TC cell (*B*) activity as a function of time and distance along the model slice. Two oscillations are initiated by focal excitation of RE cells on opposite ends of the network and 100 ms out of phase. As they propagate outward, the 2 oscillations collide, coalesce, and come into synchrony. Note that, on the cycle of activity immediately after the collision, the phase gradient varies smoothly across the network. Synaptic conductances were the same as in Fig. 7.

center of the slice where they coalesce and come into synchrony (Kim et al. 1995). On the basis of our earlier results, we hypothesized that long-range tickler connections may help to synchronize colliding oscillations. To test this hypothesis, we simulated collisions among propagating oscillations in networks with long-range and short-range tickler connections ($g_{\text{GABA-B}}$ was 31.5 and 42 nS, respectively, in these 2 networks). To simulate collisions among oscillations propagating from opposite ends of a thalamic slice (Kim et al. 1995), we initially stimulated two groups of RE cells on opposite ends of a network, 100 ms out of phase.

Figure 10, *A* and *B*, shows contour plots of the resulting RE and TC cell activity, respectively, in the network with long-range tickler connections. Figure 11, *A* and *B*, shows the corresponding plots for the network with short-range tickler connections. Activity in both networks is organized in two propagating oscillations, beginning from opposite ends of the network. In both cases, the two oscillations collide and coalesce. However, as Fig. 10 shows, in the network with long-range tickler connections, the oscillations coalesce rapidly, so that immediately after the collision the phase gradient (i.e., phase difference between neighboring cells) varies smoothly across the network. In contrast, in the network with short-range tickler connections (Fig. 11), the oscillations coalesce, but they do so more slowly, so that immediately after the collision there are still large discontinuities in the phase gradient across the network. This suggests that long-range tickler connections may indeed help to synchronize colliding oscillations.

DISCUSSION

Through a combination of computational modeling and in vitro extracellular recording, we observed the following. *1*) Activity in bicuculline-treated thalamic slices oscillates at ≈3 Hz, and these oscillations are synchronized with small phase differences over relatively large distances in VB and RE. *2*) Similar oscillations result in a network model through the previously published cycle of events; RE cells' bursts elicit slow $GABA_B$ IPSPs in TC cells, these IPSPs deinacti-

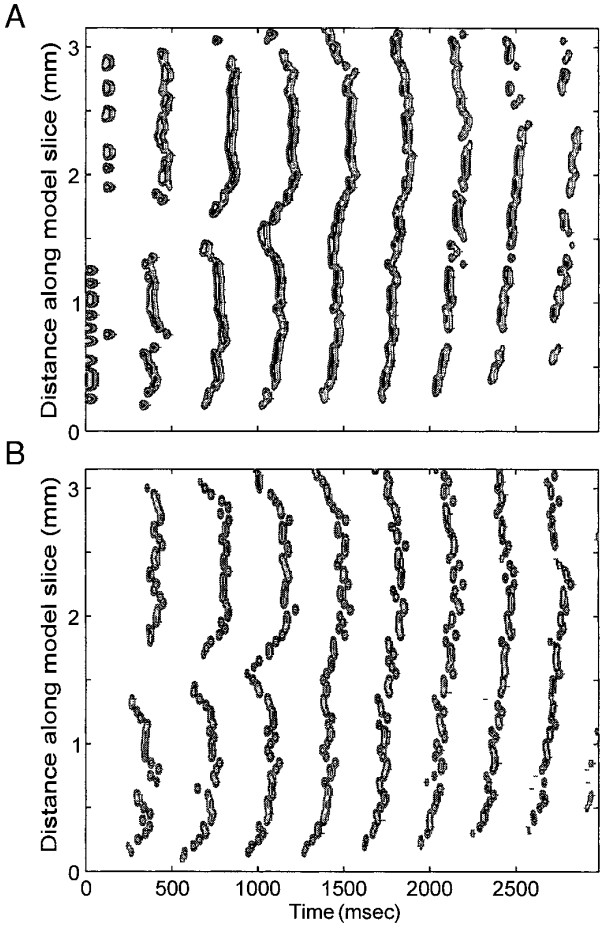

FIG. 11. Colliding oscillations in a network without long-range tickler connections. Contour plot of concurrent RE cell (*A*) and TC cell (*B*) activity as a function of time and distance along the model slice. Two oscillations are initiated by focal excitation of RE cells on opposite ends of the network and 100 ms out of phase. As they propagate outward, the 2 oscillations collide, coalesce, and come into synchrony. Note that, in contrast to Fig. 10, on the cycle of activity immediately after the collision, the phase gradient changes sharply where the 2 oscillations collided. Synaptic conductances were the same as in Fig. 8.

Downloaded from on April 2, 2015

vate I_T and are therefore followed by rebound bursts in TC cells, and TC cells' bursts elicit fast EPSPs in RE cells, producing bursts. *3*) In the network model, modest T-channel blockade reduces the duration and increases the period of these oscillations, whereas modest synaptic suppression shortens both the duration and the period of these oscillations. For some initial values of $g_{leak,K}$, CCK prolongs oscillations at low doses but curtails these oscillations at higher doses. For lower initial values of $g_{leak,K}$, all doses of CCK curtail oscillations. CCK always shortens the period of these oscillations. *4*) Focal excitation of RE cells elicits oscillations that propagate outward. By choosing $\bar{g}_{GABA\text{-}B}$ appropriately, we were able to obtains propagation speeds similar to those observed in vitro (Kim et al. 1995) in networks with either short-range or long-range tickler connections. 5) However, by using the $\bar{g}_{GABA\text{-}B}$ values that produce physiologically realistic propagation speeds, the network model with short-range tickler connections and the model with long-range connections exhibit radically dissimilar phase differences between activity at distinct locations. Only the relatively small phase differences produced by the network with long-range tickler connections are similar to those observed in vitro. Furthermore, although colliding oscillations coalesce in both networks, the colliding oscillations come into synchrony much more rapidly in the network with long-range tickler connections.

The first observation extends earlier descriptions of synchronous, ≈3-Hz intrathalamic oscillations in vitro (Bal et al. 1995a,b; Huguenard and Prince 1994; Kim et al. 1995; von Krosigk et al. 1993). Observations 2 through 4 demonstrate that our network model is consistent with a wide body of experimental observations. The final observation constitutes our main finding that, when $\bar{g}_{GABA\text{-}B}$ is chosen to reproduce the propagation speed observed in vitro (Kim et al. 1995), the network without long-range tickler connections does not reproduce the maximal phase differences we found during ≈3-Hz oscillations in vitro.

Note that this quantitative comparison between simulated phase shifts and those found experimentally is valid only insomuch as randomly activating one-third of RE cells accurately models the indirect excitation of RE cells via stimulation of internal capsule. However, the qualitative observation that long-range connections smooth phase differences during collisions between oscillations does not suffer from such limitations.

Propagation speed depends on synaptic strength and the spread of intrathalamic connections

As noted previously (Golomb et al. 1996) the speed with which synchronous ≈3-Hz oscillations propagate depends on both the synaptic conductance and the radius of connections. This has important consequences for conclusions drawn from computational models. For example, other models assumed a value for synaptic conductances and, based on that value, estimated the spread of intrathalamic projections for which model oscillations propagate at physiologically realistic speeds (Destexhe et al. 1996a; Golomb et al. 1996). In contrast, we emphasize that the $GABA_B$ synaptic conductance can be adjusted (e.g., networks with only short-range connections have $\bar{g}_{GABA\text{-}B}$ = 42 nS whereas those with both short and long-range connections have $\bar{g}_{GABA\text{-}B}$ = 31.5 nS), so that the extent of intrathalamic connectivity could increase fivefold without significantly changing the speed at which oscillations propagate. Thus we could not distinguish networks with only short-range connections from those with both short- and long-range connections just on the basis of propagation speed.

Phase differences measured in vitro also constrain network models

Because there exist multiple combinations of two parameters—$\bar{g}_{GABA\text{-}B}$ and the radius of tickler connections—that produce propagation speeds similar to those observed in vitro, we looked for an additional observable that would constrain the values of these two parameters in our network model. Casual comparison of Figs. 7 and 8 suggested that different values of these parameters that produced similar speeds could be distinguished based on the phase differences they produced during ≈3-Hz oscillations.

Phase differences across network models during propagating ≈3-Hz oscillations were studied before (Golomb et al. 1996). This study concluded that, away from edges and the wavefront, phase shifts grow linearly with distance; however, this would be true for any translation-invariant system. Furthermore, this study dealt with phase shifts that develop as the wavefront of the oscillation propagates. Because these phase shifts develop over time, they are affected by many aspects of network activity. Thus these phase shifts depend sensitively on network parameters (Golomb et al. 1996). Such complexity would make it difficult to constrain our network model based on these phase shifts.

Therefore, instead of measuring phase shifts that develop as an oscillation propagates (Golomb et al. 1996), we measured the phase shifts on the first cycle of activity after far-reaching stimulation of RE cells. As shown in RESULTS, these phase differences depend primarily on synaptic conductance and the radius of connectivity from RE to TC cells and are therefore particularly useful measurements with which to constrain the radius of RE to TC connectivity and the strength of synaptic transmission in our network model.

Long-range connections synchronize, rather than spread, oscillations

The assumption that the range of intrathalamic connectivity determines the distance over which oscillations spread per cycle and hence the speed of propagation is implicit in models of intrathalamic oscillations that use the speed of propagation to infer the spread of intrathalamic connectivity (Destexhe et al. 1996a; Golomb et al. 1996). Our observation that two networks in which the ranges of tickler cell connections differ by a factor of five may exhibit similar propagation speeds but radically different phase shifts dispels this assumption and suggests that long-range tickler connections (Cox et al. 1996) function to synchronize activity and minimize phase shifts across the network rather than to spread activity over greater distances.

Simulations of collisions between propagating oscillations also support the hypothesis that long-range tickler connections help to synchronize network activity. These simulations

Downloaded from on April 2, 2015

showed that, immediately after a collision between out-of-phase propagating oscillations, phase gradients varied smoothly across the network with long-range tickler connections but changed abruptly in the network with short-range tickler connections. Because in the former case the range of tickler connections exceeded the distance over which oscillations spread each cycle, these long-range tickler connections effectively smoothed the phase gradients between the two oscillations before they collided. However, in the latter case, the range of tickler connections was approximately the same as the distance over which oscillations spread each cycle, so these short-range tickler connections did not smooth phase gradients between the two oscillations until after they collided. Thus, long-range tickler connections that synchronize activity rather than spread activity over greater distances may contribute significantly to the smoothing of phase gradients between colliding waves.

Synchronization of activity by long-range tickler connections may have other important implications for thalamic networks. For example, suppose that cortical oscillations are driven by the arrival of nearly simultaneous waves of excitation (or inhibition) from the thalamus. Then, by reducing phase differences across the thalamic network, long-range tickler connections may enhance the ability of thalamic oscillations to entrain cortical oscillations. In this way, changes in the relative numbers of tickler and cluster cells that form during development could have profound consequences on thalamic function.

Here we have focused on the possible dynamics of thalamic networks that contain both short- and long-range RE to TC cell connections (cf. Cox et al. 1996). However, there are also regions containing exclusively long-range, diffuse RE-to-TC cell connections such as the rostral pole of the RE complex (Steriade et al. 1984). Our results may illustrate ways in which these regions can synchronize thalamic activity.

Effects of edges and finite size of the model

The edges and finite size of the model should not have created spurious conclusions because our conclusions were based on phase shifts and speeds at which oscillations propagated, neither of which was affected by the model's edges or finitude. First consider the phase shifts. We measured phase differences on the first cycle of oscillations after broad stimulation. As a result, the presence of edges could only affect TC cells <500 μm (the radius of tickler connections) from an edge. We excluded these cells when computing phase differences. Therefore the computed phase difference was unaffected by the presence of edges. In addition, the conclusions regarding phase shift were not dependent on model size as a 256-cell network (representing a standard-length slice) produced results similar to those observed in vitro only when long-range tickler connections were present.

Now consider the speed at which oscillations propagate. These oscillations were elicited by focal stimulation at the center of the model slice. Therefore the presence of edges could only affect network activity once cells within 500 μm of an edge became active. As can be seen from Figs. 7 and 8, oscillations never came within 500 μm of an edge during the first 1.5 s of propagation, the period over which we calculated the speed.

Finally, we used two 256-cell networks, representing thalamic slices of either standard length or twice the standard length, to evaluate the effects of the network's finite size and edges, respectively, on phase shifts after collisions. Like the 128-cell network, both 256-cell networks required long-range tickler connections to produce a smooth phase gradient immediately after a collision between two initially out-of-phase oscillations. Furthermore, oscillations in all three networks propagated at similar speeds.

Limitations of this model

Two shortcomings of this network model of intrathalamic oscillations are that it lacks the refractory period between oscillations observed in vitro (Kim et al. 1995) and that in the model the period of oscillations become slightly shorter as the oscillation progresses, whereas in vitro (unpublished observations) and during clinical absence seizures (Panayiotopoulos 1994) the period lengthens significantly. The first of these shortcomings might be corrected by inclusion of Ca^{2+}-dependent persistent activation of I_h in TC cells. (In addition, the progressive hyperpolarization of RE/PGN cells observed during in vitro oscillations might influence oscillation period) (Bal et al. 1995a). The h-current modulation mechanism was shown to reproduce the refractory period in earlier models (Destexhe et al. 1996a), and there is strong evidence that it contributes to refractoriness in vitro (Bal and McCormick 1996). To study how persistent activation of I_h would affect the period of oscillations, we simulated oscillations with the I_h model from a previous study (Destexhe et al. 1996a) that included Ca^{2+}-dependent persistent activation. We found that, as this persistent activation of I_h increased, the period of oscillations decreased. Thus, during an oscillation, as activation of I_h increases, the oscillation's period would gradually decrease, contrary to experimental observations.

There are also limitations on our estimates for the phase shifts on the first cycle of activity after stimulation of many RE cells. We assumed that randomly activating one-third of the RE cells in the network model is comparable with the indirect excitation of RE cells via stimulation of internal capsule in vitro. Intracellular recording has shown that such indirect excitation of RE cells evokes IPSCs in TC cells, and these IPSCs are composed of conspicuous peaks that occur at intervals of 1.5–3.6 ms, similar to the intraburst spiking frequency of RE cells (Huguenard and Prince 1994). This suggests that the evoked IPSCs are dominated by input from only one or a few bursting RE cells, i.e., only a few of the many RE cells presynaptic to one TC cell burst after stimulation of internal capsule. If this is true, then the probabilities of RE cells bursting after stimulation of internal capsule have a Poisson distribution, which has a relatively low mean and high variance, and would therefore be similar to the distribution of RE cell firing assumed in the model.

Another limitation on our estimate of phase shifts is that in the model we calculated phase shifts among the activities of individual cells, whereas in the experiment we calculated phase shifts among extracellularly recorded activities. However, because the maximum phase shifts in the networks with long- and short-range tickler connections were so dramatically different, we can say that the range of phase shifts observed in vitro

Downloaded from on April 2, 2015

is similar to that observed in the network with long-range tickler connections but is inconsistent with the range observed in the network with short-range tickler connections.

Predictions

We quantitatively compared the maximum phase difference in between the activity of TC cells after widespread stimulation of RE cells in a network model with long-range tickler connections, in a network model with short-range tickler connections, and in vitro. This comparison could be improved. The network models assumed values of $\bar{g}_{\text{GABA-B}}$ chosen to produce propagation speeds similar to those observed in vitro. However, the in vitro measurements of phase differences and propagation speeds were made in different thalamic slices, taken from different animals, by different researchers. A more rigorous test of this model would be to reproduce the propagation speed and phase differences of a single slice and any covariance of propagation speed and phase differences between slices. Predictions about how certain pharmacological manipulations should affect both the propagation speed and phase differences are as follows.

1) We found that reducing the permeability of T currents reduces the duration but lengthens the period of ≈3-Hz oscillations in the network model, consistent with the effects of T-channel blockers measured in vitro (Huguenard and Prince 1994; Smith and Huguenard 1996). Because T-channel blockers increase the threshold for rebound bursts in TC cells, which should reduce the number of TC cells recruited by propagating oscillations and lengthen the period of these oscillations, T-channel blockers should reduce the speed at which oscillations propagate. We can also use *Eq. 4* and simulations to predict how T-channel blockers will affect the maximum phase difference among TC cells (measured on the first cycle of activity after widespread stimulation of RE cells). From that equation we see that the maximum phase difference, $\Delta\phi$, should depend on the values of $n_{\min}$, the minimum number of IPSPs that occur in a TC cell and elicit a rebound burst, and $n_{\max}$, the maximum number of IPSPs that occur in a TC cell, in other words

$$\Delta\phi = \tau \ln\left[\frac{n_{\max}(1 + n_{\min}\tilde{g})}{n_{\min}(1 + n_{\max}\tilde{g})}\right] \quad (5)$$

Modest reductions in T current will increase the burst threshold in TC cells but have no effect on $n_{\min}$ or $n_{\max}$ and therefore should not affect $\Delta\phi$. Only after the T current was reduced enough to increase $n_{\min}$, the number of IPSPs necessary to elicit a rebound burst, should $\Delta\phi$ begin to decrease. This prediction was confirmed by the results of simulations, shown in Fig. 4. Reducing T-current permeabilities by ≤37.5% only reduced $\Delta\phi$ by at most 1 ms.

2) We found that suppression of synaptic strength shortens both the duration and the period of oscillations in the model network. Also, we commonly found that reductions in synaptic strength reduced the ability of the network to support propagating oscillations and would therefore predict that propagation speed should decrease with decreasing synaptic strength. Finally, we can use *Eq. 4* to predict $\Delta\phi$ after decreases in synaptic strength. Because the minimum IPSP required to elicit a rebound burst is independent of $\tilde{g}$ (synaptic strength), the quantity $n_{\min}\tilde{g}$ should remain constant so that $\Delta\phi$ depends on $n_{\max}$

$$\Delta\phi = \tau \ln\left[\frac{n_{\max}\tilde{g}}{1 + n_{\max}\tilde{g}}\right] - \text{constant} \quad (6)$$

Thus, $\Delta\phi$ should decrease with decreasing $\tilde{g}$, i.e., the maximum phase difference should decrease as synaptic transmission is suppressed. This general trend was observed in simulations, the results of which are plotted in Fig. 5. To test these predictions in vitro, synaptic transmission could suppressed either presynaptically, with N- or P/Q-type Ca^{2+} channel blockers, or postsynaptically, by a combination of AMPA and $GABA_B$ receptor antagonists. Assuming that intraslice variability results from differences in the extent of functional connectivity (Cox et al. 1997b), we would predict that the duration, period, propagation speed, and maximum phase shift on the first cycle of activity should all covary (because they all decrease as the strength of synaptic transmission decreases). Of course, to measure such covariance between slices, other factors, especially the number of RE cells activated by the initial stimulus, should be kept as constant as possible.

3) The results of simulations, shown in Fig. 6, predict that reducing the K^+ leak conductance of RE cells, by applying CCK, reduces both the period of oscillations and $\Delta\phi$. Both of these effects can be explained by assuming that depolarizing RE cells reduces the deinactivation of I_{Ts} between bursts. Subsequently, RE cells' burst become shorter and evoke weaker IPSPs in TC cells. As a result, the effects of CCK on the period of oscillations and $\Delta\phi$ are analogueous to the corresponding effects of suppressing synaptic strength.

4) Waning of oscillations in the model depends on activation of presynaptic receptors. This is a different mechanism than that proposed by Bal and McCormick (1996). If it were possible to pharmacologically inhibit presynaptic but not postsynaptic $GABA_B$ receptors, we would predict that such a manipulation would prolong oscillations. At this point there are no such specific $GABA_B$ antagonists currently available.

A second test of the model, distinct from validating the predicted effects of pharmacological manipulations, would be studying the heterogeneity of RE to TC projections, which this model assumes. One example would be to verify the heterogeneity in the range of RE to TC projections, which was observed anatomically (Cox et al. 1996) by using physiological methods. This could be done by focally stimulating a small group of RE cells (e.g., by blocking excitatory transmission and electrically stimulating RE cells or direct application of glutamate onto a small group of RE cells) and measuring the responses of TC cells at different locations. On the basis of the RE to TC projections assumed by the model, we would predict that focal stimulation of RE cells should produce strong inhibition within a central radius of ≈100 μm and weaker inhibition within a larger radius of ≈500 μm.

Finally, our simulations predict that collisions among propagating oscillations should be accompanied by relatively smooth phase gradients, such as those shown in Fig. 10, not phase gradients that change abruptly, as shown in Fig. 11.

APPENDIX A: A MODEL PARAMETERS

Intrinsic currents

As in earlier studies (Hodgkin and Huxley 1952; Huguenard and McCormick 1992), we assumed that each intrinsic current

Downloaded from on April 2, 2015

was composed of many equivalent ion channels, each channel was comprised of at least one gate, and all of the gates comprising an individual channel must be open for the channel to conduct current. This leads to the same generic formalism for all voltage-dependent intrinsic currents

$$\hat{g} = m^M h^N \quad (A1)$$

where $\hat{g}$ is the current's condutance or permeability as a fraction of its maximum conductance or permeability.

We used Ohm's law to calculate non-Ca^{2+} currents, i.e.,

$$I = g_{max}\hat{g}(V_m - E_{eq}) \quad (A2)$$

where V_m is the membrane potential and g_{max} and E_{eq} are the current's maximum conductance and equilibrium potential, respectively. For the low-threshold Ca^{2+} currents, I_T and I_{Ts}, we used the constant field equation

$$I = \hat{g}Pz^2\frac{V_m F^2}{RT}\frac{[Ca^{2+}]_i - [Ca^{2+}]_o e^{-zFV_m/RT}}{1 - e^{-zFV_m/RT}} \quad (A3)$$

where P is the maximum permeability, z is 2 (the valence of Ca^{2+}), $[Ca^{2+}]_i$ = 240 nM and $[Ca^{2+}]_o$ = 2 mM are the concentration of Ca^{2+} inside and outside of the cell, respectively, F is Faraday's constant, and R is the universal gas constant.

The kinetics of I_{Na} and I_K were taken from Traub and Miles (1991), and the maximum conductances were adjusted to give action potentials of realistic height and duration.

To model I_T in TC cells, we used the two-variable (m^2h) kinetic scheme of Huguenard and McCormick (1992), in which all rate constants were temperature corrected by using a Q_{10} = 2.5. We set the maximum permeability of the T current, P_T, to 50×10^{-9} cm^3/s (at the simulation temperature of 37°C). This permeability falls within the range of values observed in intact cells (McCormick and Huguenard 1992) and was chosen so that both the number of spikes per burst during bicuculline-induced synchronized oscillations and the change in the duration of these oscillations after partial blockade of T-channels were similar in simulations and experiments.

We modeled I_h in TC cells by using the single variable (m) kinetic scheme of Huguenard and McCormick (1992), in which all rate constants were temperature corrected with a Q_{10} = 3. We set the maximum h-current conductance to 20 $\mu S/cm^2$. This was the same value used in a previous model (Destexhe et al. 1996a) and was sufficient to produce characteristic oscillations in isolated TC cells (not shown) (see McCormick and Huguenard 1992). As in previous simulations (Destexhe et al. 1996a; Huguenard and McCormick 1992; McCormick and Huguenard 1992) the h-current equilibrium potential was −40 mV.

TC cells had a leak conductance of 24 $\mu S/cm^2$, corresponding to an input resistance of ~140 MΩ, characteristic of TC cells in a deafferented slice. At a typical resting membrane potential of −63 mV, T-current activation and inactivation reached a steady state, producing a significantly depolarizing ''window current.'' To balance this depolarizing window current, the leak current's equilibrium potential had to be hyperpolarized relative to the resting membrane potential. We found that setting E_{leak} to −75 mV produced a resting membrane potential of −63 mV. Therefore the E_{leak} of each TC cell was drawn from a normal distribution with a mean of −75 mV and SD of 2 mV. We used a distribution of E_{leak} values to approximate the variation of cellular excitability in vitro and eliminate some spurious solutions that might have been produced by nonphysiological symmetry in the network.

We modeled I_{Ts} in RE cells with a two-variable (m^2h) kinetic scheme developed earlier (Destexhe et al. 1996b) and temperature corrected all rate constants with Q_{10} = 2.5. As for I_T, the maximum permeability of I_{Ts}, 20×10^{-9} cm^3/s (at 37°C), was chosen so that both the number of spikes per burst during bicuculline-induced synchronized oscillations and the change in the duration of these oscillations after partial blockade of T-channels were similar in simulations and experiments.

RE cells had a leak conductance of 25 $\mu S/cm^2$. We found that a leak current equilibrium potential of −85 mV in an RE cell was sufficiently hyperpolarized that I_{Ts} would deinactivate between bursts and the cell would not burst spontaneously. Therefore the E_{leak} of each RE cell was drawn from a normal distribution with a mean of −85 mV and SD of 2 mV.

Time course of postsynaptic $GABA_B$ currents

Like voltage-dependent intrinsic currents that were modeled by using *Eq. A1*, the time course of postsynaptic $GABA_B$ currents was modeled as the product of an activation function, $m(t)$, and an inactivation function, $h(t)$. On the basis of in vitro measurements made in the dentate gyrus at 34°C (Otis et al. 1993), $m(t)$ has a monoexponential rise (time constant = 45.2 ms) and is raised to the fourth power, whereas the inactivation function, $h(t)$, consists of a biexponential decay (fast decay: time constant = 110.2 ms, relative weight = 84%; slow decay: time constant = 516.2 ms, relative weight = 16%) and is raised to the first power. The time constants were temperature corrected by using a Q_{10} of 2.2.

Postsynaptic $GABA_B$ receptor occupancy

To calculate the fraction of occupied postsynaptic $GABA_B$ receptors at a synapse, we assumed that the fraction of $GABA_B$ receptors occupied because of an earlier $GABA_B$ response equaled the number of $GABA_B$ receptors activated on that response up until that response's peak and thereafter decayed with the same time course as the $GABA_B$ current, i.e.,

$$\text{Fraction of occupied } GABA_B \text{ receptors} = \sum_i R_i \alpha(t - t_i) \quad (A4)$$

where the sum is taken over all previous $GABA_B$ responses at the same synapse (indexed by i), R_i is the fraction of receptors that were activated by $GABA_B$ response i, t is time, $GABA_B$ response i occurred at time t_i, and $\alpha(t)$ is $m^4(t)h(t)$ if $t > t_{peak}$ and *1* otherwise [$m(t)$ and $h(t)$ are the activation and inactivation functions, respectively, for the $GABA_B$ current].

Probabilistic release and paired-pulse depression

Whenever a presynaptic RE cell spiked, it released GABA from a release site located on synapse i with probability p_i. In accordance with paired-pulse depression of $GABA_B$ responses, p_i at time t was given by

$$p_i(t) = \bar{p}\prod_{t_j}[1 - k(t - t_j)n_i(t_j)] \quad (A5)$$

where the product is taken over all previous spikes at the same synapse (indexed by j), spike j occurred at time t_j, $\bar{p}$, the maximum probability of release, was 0.06 (Cox et al. 1997b), $k(t)$ is the amplitude of paired-pulse depression caused by transmitter release that occurred t milliseconds ago, and $n_i(t)$ represents the fraction of sites at synapse i that released transmitter at time t. The amplitude of paired-pulse depression because of a single spike, $k(t)$, reached a peak value of 0.1 and had a time course similar to the that of the $GABA_B$ response. The time course of paired-pulse depression was also the product of a monoexponential rise (time constant = 24.3 ms) raised to the fourth power and a biexponential decay (fast decay: time constant = 53.5 ms, relative weight = 47%; slow decay: time constant = 4,191 ms, relative weight = 53%) (Otis et al. 1993). These time constants were temperature corrected by using a Q_{10} of 2.2.

Thus the fraction by which the probability of transmitter release

Downloaded from on April 2, 2015

decreases after each previous presynaptic spike, $k(t)n$, is proportional to the fraction of sites that released after that spike. In this way, we do not track the probability of release from each individual release site. Instead, we assume that release from one site subsequently reduces the probability of release from all sites at the same synapse and that $k(t)$ describes the time course of this effect.

Postsynaptic $GABA_B$ conductance

The total postsynaptic $GABA_B$ conductance on a TC cells, $g_{\text{GABA-B}}$, was distributed between tickler and cluster connections based on the following observations:

1) Anatomic studies found that the number of RE cells with cluster connections (cluster cells) and with tickler connections (tickler cells) are roughly equal (Cox et al. 1996).

2) Paired intracellular recordings from RE cells in thalamic RE nucleus (RE) and TC cells in VB found that the average IPSC amplitude elicited by a cluster connection is ~10 times larger than that elicited by an average tickler connection (Cox et al. 1997b).

3) Paired intracellular recordings from RE cells in RE and TC cells in VB found similar numbers of cluster and tickler connections (Cox et al. 1997b).

These intracellular recordings sampled VB and RE cells over regions smaller than a cluster cell's axonal arborization (Cox et al. 1997b). Therefore, assuming that this study sampled equal numbers of cluster and tickler cells (reasonable given the first observation), the third observation provides indirect evidence that, within a small region of VB, a cluster cell and a tickler cell contact similar numbers of postsynaptic cells. Assuming that this is true, because tickler connections extend over a much greater distance than do cluster connections, one TC cell should receive many more tickler connections than cluster connections; the ratio of tickler to cluster connections on a postsynaptic cell will be approximately equal to the ratio between the area of the axonal arborization of a tickler cell and that of a cluster cell.

To represent the weaker efficacy but greater convergence of tickler connections, the ratio between $GABA_B$ conductance postsynaptic to tickler connections and that postsynaptic to cluster connections was

$$\frac{\bar{g}_{\text{GABA-B}}(\text{tickler})}{\bar{g}_{\text{GABA-B}}(\text{cluster})} = \left(\frac{\text{amplitude of tickler ipsc}}{\text{amplitude of cluster ipsc}}\right)\left(\frac{\text{area of tickler cell arbor}}{\text{area of cluster cell arbor}}\right) \quad (A6)$$

In networks with tickler connections that extended over the same radius as cluster connections, we still weighted tickler connections disproportionately so that the ratio between the $GABA_B$ conductance postsynaptic to tickler connections and that postsynaptic to cluster cells was the same as in the other networks (in which tickler connections extended over a much larger radius). Within each network, every $GABA_B$ connection of a given type (tickler or cluster) had the same postsynaptic conductance, so, as in a previous model (Golomb et al. 1996), cells at the edges of the slice, which were postsynaptic to fewer connections, did not receive their full complement of $GABA_B$ conductance.

Total synaptic input conductances

The total synaptic conductance on a TC cell is given by

$$\text{Total synaptic input to a TC cell} = \frac{\bar{g}_{\text{GABA-B}}(\text{tickler})}{N_{\text{tickler}}} \sum_i \sum_j R_{ij} m^4(t - t_{ij}) h(t - t_{ij}) + \frac{\bar{g}_{\text{GABA-B}}(\text{cluster})}{N_{\text{cluster}}} \sum_k \sum_l R_{kl} m^4(t - t_{kl}) h(t - t_{kl}) \quad (A7)$$

where N_{tickler} is the total number of tickler synapses onto the TC cell, i indexes RE cells that make a tickler synapse onto the TC cell, j indexes spikes in those presynaptic RE cells, R_{ij} and t_{ij} are the fraction of postsynaptic receptors activated by and time of the jth spike in presynaptic RE cell i, l indexes RE cells that make a cluster synapse onto the TC cell, N_{cluster} is the total number of cluster synapses onto the TC cell, k indexes spikes in those presynaptic RE cells, R_{kl} and t_{kl} are the fraction of postsynaptic receptors activated by and time of the lth spike in presynaptic RE cell k, and $m(t)$ and $h(t)$ are the activation and inactivation functions for postsynaptic $GABA_B$ currents, described earlier.

Similarly, the total synaptic conductance on an RE cell is given by

$$\text{total input conductane on an RE cell} = \frac{\bar{g}_{\text{AMPA}}}{N} \sum_i R_i(t) \quad (A8)$$

where N is the total number of AMPA synapses onto the RE cell, i indexes TC cells presynaptic to the RE cell, and $R_i(t)$ is the fraction of AMPA receptors postsynaptic to TC cell i that are active at time t evolves according to *Eq. 3*.

Calculating the speed of propagation in the network model

We used the same method as an earlier study (Golomb et al. 1996) to calculate the speed at which oscillations propagated in the network model. To calculate the speed of propagation in a particular direction, e.g., to the right, consider the subset of TC cells that spiked before any of their neighbors to the right spiked. We performed linear regression on the locations of these TC cells and the times of their first spikes and used the slope of the resulting best-fit line as the speed of propagation for oscillations in the network model.

APPENDIX B

Maximum phase shift

Assume that every RE cell burst activates the same conductance in a postsynaptic TC cell. Let $g_{\text{GABA-B}}$ represent this conductance, normalized by the passive conductance of the TC cell, and n represent the number of active RE cells presynaptic to the TC cell. Then the total $GABA_B$ conductance activated in the TC cell will be $ng_{\text{GABA-B}}$. Assume also that all presynaptic RE cells burst simultaneously and that IPSPs decay monoexponentially with a time constant of $\tau_{\text{GABA-B}}$. During an IPSP, the time constant for the h current, τ_m, is >600 ms (Huguenard and McCormick 1992). Because τ_m and $\tau_{\text{GABA-B}}$ are both at least an order of magnitude longer than the membrane time constant, we can assume that changes in the membrane potential, V_m, are ''slaved'' to changes in the h current or IPSC. Thus, as the $GABA_B$ postsynaptic potential decays, V_m will be approximately

$$V_m = \frac{m\bar{g}_h E_h + g_{\text{leak}} V_{\text{rest}} + g_{\text{GABA-B}} e^{-t/\tau_{\text{GABA-B}}} E_{\text{GABA-B}}}{m\bar{g}_h + g_{\text{leak}} + g_{\text{GABA-B}} e^{-t/\tau_{\text{GABA-B}}}} \quad (B1)$$

where m, $\bar{g}_h$, and E_h are the activation, maximum conductance, and reversal potential, respectively, of the h current. To derive *Eq. 4* we set V_m equal to the burst threshold, θ

$$\theta = \frac{m\bar{g}_h E_h + g_{\text{leak}} V_{\text{rest}} + g_{\text{GABA-B}} e^{-t_{\text{burst}}/\tau_{\text{GABA-B}}} E_{\text{GABA-B}}}{m\bar{g}_h + g_{\text{leak}} + g_{\text{GABA-B}} e^{-t_{\text{burst}}/\tau_{\text{GABA-B}}}} \quad (B2)$$

where t_{burst} is the time at which the burst threshold is crossed. Thus we are approximating the sigmoidal activation function for I_T by a step function and assuming that I_T is deactivated for $V_m < \theta$ and that I_T initiates a burst for $V_m \geq \theta$. Now, because $\tau_m > 600$ ms, we assume that the h-current conductance, $m\bar{g}_h$, remains constant.

Downloaded from on April 2, 2015

We include this simplified h current in the ''effective'' passive conductance by making the substitutions

$$E_{\text{pas}} = \frac{m\bar{g}_{\text{h}}E_{\text{h}} + g_{\text{leak}}V_{\text{rest}}}{m\bar{g}_{h} + g_{\text{leak}}} \quad \text{(B3)}$$

$$g_{\text{pas}} = m\bar{g}_{\text{h}} + g_{\text{leak}} \quad \text{(B4)}$$

Then dividing the numerator and denominator of the right-hand side of *Eq.* B*2* by g_{pas} gives

$$\theta = \frac{E_{\text{pas}} + \tilde{g}e^{-t/\tau_{\text{GABA-B}}}E_{\text{GABA-B}}}{1 + \tilde{g}e^{-t/\tau_{\text{GABA-B}}}} \quad \text{(B5)}$$

where $\tilde{g} = g_{\text{GABA-B}}/g_{\text{pas}}$. Solving *Eq.* B*5* for t_{burst} yields *Eq. 4*.

We thank B. Yue for assistance with the extracellular recording experiments.

This work was supported by National Institute of Neurological Disorders and Stroke Grants NS-06477 and NS-34774 and the Pimley Research Funds.

Address reprint requests to J. R. Huguenard.

Received 6 October 1997; accepted in final form 16 June 1998.

REFERENCES

AGMON, A., YANG, L. T., JONES, E. G., AND O'DOWD, D. K. Topological precision in the thalamic projection to neonatal mouse barrel cortex. *J. Neurosci.* 15: 549–561, 1995.

BAL, T. AND MCCORMICK, D. A. What stops synchronized thalamocortical oscillations? *Neuron* 17: 297–308, 1996.

BAL, T., VON KROSIGK, M., AND MCCORMICK, D. A. Role of the ferret perigeniculate nucleus in the generation of synchronized oscillations in vitro. *J. Physiol. (Lond.)* 483: 665–685, 1995a.

BAL, T., VON KROSIGK, M., AND MCCORMICK, D. A. Synaptic and membrane mechanisms underlying synchronized oscillations in the ferret lateral geniculate nucleus in vitro. *J. Physiol. (Lond.)* 483: 641–663, 1995b.

BURNS, B. D. Some properties of the cat's isolated cerebral cortex. *J. Physiol. (Lond.)* 111: 50–68, 1950.

CONTRERAS, D., DESTEXHE, A., SEJNOWSKI, T. J., AND STERIADE, M. Control of spatiotemporal coherence of a thalamic oscillation by corticothalamic feedback. *Science* 274: 771–774, 1996.

COX, C. L., HUGUENARD, J. R., AND PRINCE, D. A. Cholecystokinin depolarizes rat thalamic reticular neurons by suppressing a K^+ conductance. *J. Neurophysiol.* 74: 990–1000, 1995.

COX, C. L., HUGUENARD, J. R., AND PRINCE, D. A. Heterogeneous axonal arborizations of rat thalamic reticular neurons in the ventrobasal nucleus. *J. Comp. Neurol.* 366: 416–430, 1996.

COX, C. L., HUGUENARD, J. R., AND PRINCE, D. A. Peptidergic modulation of intrathalamic circuit activity in vitro: actions of cholecystokinin. *J. Neurosci.* 17: 70–82, 1997a.

COX, C. L., HUGUENARD, J. R., AND PRINCE, D. A. Nucleus reticularis neurons mediate diverse inhibitory effects in thalamus. *Proc. Natl. Acad. Sci. USA* 94: 8854–8859, 1997b.

DESTEXHE, A., BAL, T., MCCORMICK, D. A., AND SEJNOWSKI, T. J. Ionic mechanisms underlying synchronized oscillations and propagating waves in a model of ferret thalamic slices. *J. Neurophysiol.* 76: 2049–2070, 1996a.

DESTEXHE, A., CONTRERAS, D., STERIADE, M., SEJNOWSKI, T. J., AND HUGUENARD, J. R. In vivo, in vitro and computational analysis of dendritic calcium currents in thalamic reticular neurons. *J. Neurosci.* 16: 169–185, 1996b.

DESTEXHE, A. AND SEJNOWSKI, T. J. G protein activation kinetics and spillover of gamma-aminobutyric acid may account for differences between inhibitory responses in the hippocampus and thalamus. *Proc. Natl. Acad. Sci. USA* 92: 9515–9519, 1995.

GOLOMB, D., WANG, X. J., AND RINZEL, J. Propagation of spindle waves in a thalamic slice model. *J. Neurophysiol.* 75: 750–769, 1996.

GRAY, C. Synchronous oscillations in neuronal systems: mechanisms and functions. *J. Comp. Neurosci.* 1: 11–38, 1994.

HINES, M. AND CARNEVALE, N. T. The NEURON simulation environment. *Neural Comp.* 9: 1179–1209, 1997.

HODGKIN, A. L. AND HUXLEY, A. F. A quantitative description of membrane current and its application to conduction and excitation in nerve. *J. Physiol. (Lond.)* 117: 500–544, 1952.

HUGUENARD, J. R. AND MCCORMICK, D. A. Simulation of the currents involved in rhythmic oscillations in thalamic relay neurons. *J. Neurophysiol.* 68: 1373–1383, 1992.

HUGUENARD, J. R. AND PRINCE, D. A. Intrathalamic rhythmicity studied in vitro: nominal T current modulation causes robust anti-oscillatory effects. *J. Neurosci.* 14: 5485–5502, 1994.

HUGUENARD, J. R. AND PRINCE, D. A. Basic mechanisms of epileptic discharges in the thalamus. In: *Thalamus*, edited by M. Steriade, E. G. Jones, and D. A. McCormick, Oxford: Elsevier Science, 1997, vol. 2, p. 295–330.

IDE, L. S. The fine structure of the perigeniculate nucleus in the cat. *J. Comp. Neurol.* 210: 317–334, 1982.

JONES, E. G. *The Thalamus*. New York: Plenum, 1985.

KIM, U., BAL, T., AND MCCORMICK, D. A. Spindle waves are propagating synchronized oscillations in the ferret LGNd in vitro. *J. Neurophysiol.* 74: 1301–1323, 1995.

LÜBKE, J. Morphology of neurons in the thalamic reticular nucleus (TRN) of mammals as revealed by intracellular injections into fixed brain slices. *J. Comp. Neurol.* 329: 458–471, 1993.

MCCORMICK, D. A. AND HUGUENARD, J. R. A model of the electrophysiological properties of thalamocortical relay neurons. *J. Neurophysiol.* 68: 1384–1400, 1992.

MITROFANIS, J. AND GUILLERY, R. W. New views of the thalamic reticular nucleus in the adult and developing brain. *Trends Neurosci.* 16: 240–245, 1993.

MORISON, R. S. AND BASSET, D. L. Electrical activity of the thalamus and basal ganglia in decorticate cats. *J. Neurophysiol.* 8: 309–314, 1945.

OTIS, T. S., DE KONINCK, Y., AND MODY, I. Characterization of synaptically elicited GABAB responses using patch-clamp recordings in rat hippocampal slices. *J. Physiol. (Lond.)* 463: 391–407, 1993.

PANAYIOTOPOULOS, C. P. The clinical spectrum of typical absence seizures and absence epilepsies. In: *Idiopathic Generalized Epilepsies: Clinical, Experimental and Genetic Aspects*, edited by A. Malafosse, P. Genton, E. Hirsch, C. Marescaux, D. Broglin, and R. Bernasconi. London: John Libbey, 1994, p. 75–85.

SCHEIBEL, M. E. AND SCHEIBEL, A. B. The organization of the nucleus reticularis thalami: a Golgi study. *Brain Res.* 1: 43–62, 1966.

SMITH, S. D. AND HUGUENARD, J. R. The specific T-type Ca^{2+} channel blocker U92032 reduces synchronous phasic discharge in thalamus (Abstract). *Epilepsia* 37: S5:116, 1996.

SOHAL, V. S. AND HUGUENARD, J. R. Localization of CCK receptors in thalamic reticular neurons: a modeling study. *J. Neurophysiol.* 79: 2820–2824, 1998.

SPREAFICO, R., BATTAGLIA, G., AND FRASSONI, C. The reticular thalamic nucleus (RTN) of the rat: cytoarchitectural, Golgi, immunocytochemical, and horseradish peroxidase study. *J. Comp. Neurol.* 304: 478–490, 1991.

STERIADE, M., PARENT, A., AND HADA, J. Thalamic projections of nucleus reticularis thalami of cat: a study using retrograde transport of horseradish peroxidase and fluorescent tracers. *J. Comp. Neurol.* 229: 531–547, 1984.

STERIADE, M., MCCORMICK, D. A., AND SEJNOWSKI, T. J. Thalamocortical oscillations in the sleeping and aroused brain. *Science* 262: 679–685, 1993.

STERIADE, M., DESCHÊENES, M., DOMICH, L., AND MULLE, C. Abolition of spindle oscillations in thalamic neurons disconnected from nucleus reticularis thalami. *J. Neurophysiol.* 54: 1473–1497, 1985.

TRAUB, R. D. AND MILES, R. *Neuronal Networks of the Hippocampus.* Cambridge, UK: Cambridge Univ. Press, 1991.

ULRICH, D. AND HUGUENARD, J. R. $GABA_B$ receptor-mediated responses in GABAergic projection neurones of rat nucleus reticularis thalami in vitro. *J. Physiol. (Lond.)* 493: 845–854, 1996a.

ULRICH, D. AND HUGUENARD, J. R. Gamma-aminobutyric acid type B receptor-dependent burst-firing in thalamic neurons: a dynamic clamp study. *Proc. Natl. Acad. Sci. USA* 93: 13245–13249, 1996b.

ULRICH, D. AND HUGUENARD, J. R. Spindle like oscillations in rat somatosensory thalamus in vitro. *Neurosci. Abstr.* 23: 573, 1997.

VON KROSIGK, M., BAL, T., AND MCCORMICK, D. A. Cellular mechanisms of a synchronized oscillation in the thalamus. *Science* 261: 361–364, 1993.

WANG, X. J. AND RINZEL, J. Alternating and synchronous rhythms in reciprocally inhibitory model neurons. *Neural Comp.* 4: 84–97, 1992.

Downloaded from on April 2, 2015